Measurements of Bunch Motion Due to the Longitudinal Dipole-Coupled Bunch Instability at the Cornell Electron-Positron Storage Ring

Robert Holtzapple and Michael Billing

Laboratory of Nuclear Studies, Cornell University, Ithaca, NY 14853

Abstract

In the past a longitudinal dipole-coupled bunch instability had limited high current operation at CESR and resulted in a degradation of luminosity performance. A longitudinal feedback system successfully damps this instability and the exchange of superconducting RF cavities for normal conducting RF cavities in CESR has further reduced the instability's strength. A description of the longitudinal dynamics with the instability present are described in this paper as well as detailed measurements of the instability using a dual-axis synchroscan streak camera. The measurements were made on single trains of bunches, multiple trains, and colliding beams. These measurements give a characterization of the instabilities degradation of luminosity, modes of oscillation, and bunch distribution changes.

I. Introduction

To achieve high luminosity, CESR is operated with multiple bunches. Under present conditions, there are up to nine trains of bunches, with up to five bunches in each train, for a maximum of 45 positron and electron bunches (fig.1). One limitation to high luminosity is a longitudinal dipole-coupled bunch instability (LDCBI) which occurs when multiple bunches are present. The LDCBI was first noted during operation with nine trains of two bunches in CESR. At the instability threshold, a rapid growth of the spectral lines at the synchrotron sidebands of the rotation harmonics was observed. The growth of amplitude for the spectral lines depends upon the spacing of the trains and bunches and it is the indication for when the instability threshold is exceeded. The threshold of the LDCBI depends on the spacing between bunches and the number of bunches in each train. The LDCBI degrades the machine luminosity and, at high current, is responsible for beam loss.

To combat the LDCBI, two modifications were made: 1) a low Q, 1.1 GHz. accelerating cavity is used as a longitudinal feedback cavity to damp the LDCBI. 2) To increase the current threshold and reduce the effect of the LDCBI, four single cell niobium superconducting RF cavities have been installed in CESR replacing twenty cells of normal conducting RF cavaties. The superconducting RF cavities have more strongly damped higher order modes than the previous normal conducting RF cavities[1]. Measurements of the LDCBI at CESR have been made using a dual sweep synchroscan streak camera. The change in the characteristics of the instability due to the superconducting RF cavities will be discussed. A previous characterization of the LDCBI were performed with a single sweep steak camera with the normal conducting RF cavities. A single sweep streak camera can only measure single bunch dynamics; therefore, detailed information of bunch oscillations has not been previously measured[2].

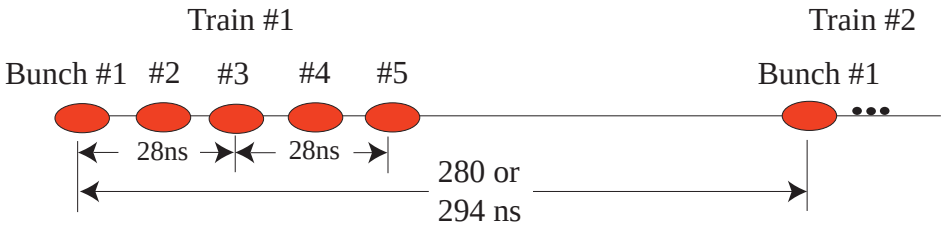

FIG. 1 (color). There are nine trains of bunches in CESR. Each train is separated by 280 or 294 ns and can have up to five bunches per train. The spacing between bunches is 14 ns.

II. Dipole-Mode Longitudinal Coupled Bunch Instability and the Longitudinal Dynamics of CESR

Several aspects of the longitudinal dipole-coupled bunch instability are presented in the section. The measurements made for this paper do not provide enough information to make a complete theoretical model of multiple bunch longitudinal dynamics in CESR, but instead, several aspects of longitudinal dynamics observed in the presence of the LDCBI will be presented. A good starting place is the description of single particle longitudinal dynamics, followed by a description of multiple bunch dynamics that relate to the instability such as time oscillation, bunch distributions, and luminosity degradation.

(a) Single Particle Longitudinal Dynamics

For a single particle, ignoring collective effects (low current), the longitudinal phase space for electrons, or positrons in a circular accelerator exhibit motion described by the following differential equations[3],

$$\frac{d\tau}{dt} = -\alpha\delta \tag{1}$$

$$\frac{d\delta}{dt} = \frac{1}{E_0 T_0}\left\{eV(\tau) - U_{rad}(\delta)\right\} \tag{2}$$

where τ and δ are the temporal and fractional energy deviations of a particle with respect to the synchronous particle, where α is the momentum compaction factor, T_0 is the circulation time, E_0 is the beam energy, $eV(\tau) - U_{rad}(\delta)$, is the net energy gain from the RF voltage and synchrotron radiation losses. From these equations and the assumption that the particles being described radiate very many small quanta during their circuit around the ring, the particles in the bunch will have a Gaussian distribution in both phase space coordinates,

$$f_0(\tau,\delta) = \frac{1}{2\pi\sigma_\tau\sigma_\delta}\exp\left(-\frac{\tau^2}{2\sigma_\tau^2} - \frac{\delta^2}{2\sigma_\delta^2}\right)$$

where the standard deviations in both coordinates are related by the synchrotron oscillation angular frequency, ω_s,

$$\omega_s = \sqrt{\frac{\alpha e\dot{V}}{E_0 T_0}} \quad \sigma_\tau = \frac{\sigma_\delta}{\omega_s}$$

where $\dot{V} = \frac{dV_{RF}}{dt}$. The standard deviation bunch length in a storage ring is[3]

$$\sigma_\tau = \frac{\alpha}{\omega_s}\sqrt{C_q E_0^2\left(\frac{I_3}{2I_2 + I_4}\right)}$$

where I_2, I_3 and I_4 are the synchrotron integrals, and C_q is the constant of $3.84\text{x}10^{-13}$m. The synchrotron integrals and longitudinal parameters are denoted in table 1 for the conditions under which the measurements were made.

I_1	8.53m	σ_E/E	$6.728\text{x}10^{-4}$
I_2	$1.047\text{x}10^{-1}\text{m}^{-1}$	σ_Z	$1.719\text{x}10^{-2}$m
I_3	$2.300\text{x}10^{-3}\text{m}^{-2}$	E_0	5.289 GeV
I_4	$1.482\text{x}10^{-3}\text{m}^{-1}$	T_0	$2.56\text{x}10^{-6}$ sec
ν_{rf}	500MHz	α	$1.11\text{x}10^{-2}$
U_0	1.14MeV	V_{rf}	6.00MV

Table 1. The synchrotron integral and longitudinal parameters for CESR.

The longitudinal phase space (τ,δ) is described by Hamiltonian dynamics. The Hamiltonian is determined from Eq. 1 and 2 where $eV(\tau) - U_{rad}(\delta)$ is the energy gained/lost due to synchrotron radiation, the RF accelerating voltage, longitudinal wake potential, and any external time-dependent voltage, eV_{ext}, which changes the energy of the particles. The function $eV(\tau) - U_{rad}(\delta)$ is given by

$$eV(\tau) - U_{rad}(\delta) = eV_{rf}\sin(\omega_{rf}\tau + \phi) - U_{rad} + eV_{ext}$$

and substituting $eV(\tau) - U_{rad}(\delta)$ back into the second equation gives

$$\frac{d\delta}{dt} = \frac{1}{T_0 E_0}\left[eV_{rf}\sin(\omega_{rf}\tau + \phi) - U_{rad} + eV_{ext}\right].$$

The two differential equations can be used to find the Hamiltonian $H = H(\delta, \tau, t)$ which describes the longitudinal motion of the bunch,

$$H(\delta,\tau,t) = \frac{\alpha^2\delta^2}{2} - \frac{\alpha}{T_0 E_0}\left\{(U_{rad} - eV_{ext})\tau + \frac{eV_{rf}}{\omega_{rf}}\cos(\omega_{rf}\tau + \phi)\right\}.$$

The phase potential, $\Phi(\tau)$, for the RF bucket is

$$\Phi(\tau) = \frac{-\alpha}{T_0 E_0}\left((U_{rad} - V_{ext})\tau + \frac{eV_{rf}}{\omega_{rf}}\cos(\omega_{rf}\tau + \phi)\right).$$

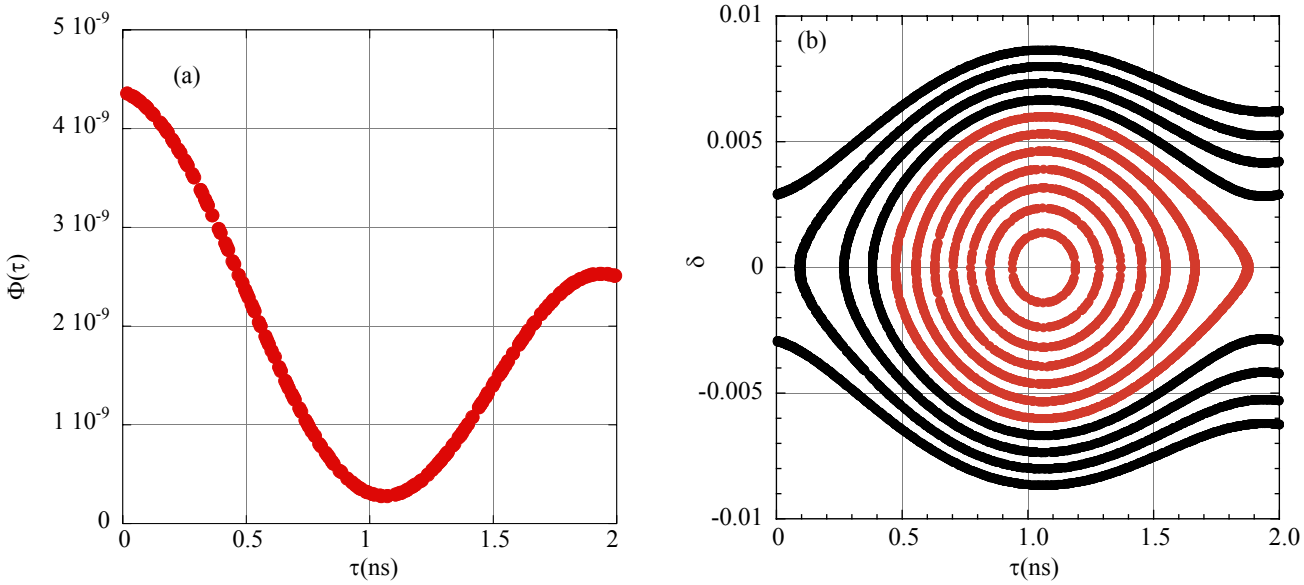

FIG. 2 (color). (a) The normalized potential energy ignoring the external potential term and (b) the longitudinal phase space for the CESR RF bucket using the parameters in table 1.

The shape of the RF bucket is calculated by varying the τ and δ coordinates while keeping the Hamiltonian fixed. The potential energy and RF bucket is plotted in fig. 2. Several features can be pointed out: 1) The asymmetry in the potential energy is due to the average synchrotron radiation loss. 2) The red lines represent the stable phase space trajectories within the RF bucket plotted for particles having equal increments in fractional energy error. The separatrix is the phase space trajectory having the maximum amplitude for a captured particle. 3) The black lines represent the trajectories of particles that will not be captured in the RF bucket. Ignoring radiation damping, a particle that is injected onto one of these trajectories will remain on that trajectory as it moves in phase space.

In a storage ring, which has synchrotron radiation losses dominated by the emission of a large number of small quanta, the equilibrium distribution is Gaussian in fractional energy deviation and temporal deviation as mentioned above. If one were to apply an external periodic voltage (V_{ext}) varying slowly in time, the phase space trajectories would become time modulated. Since this slowly varying modulating voltage can be viewed as adding to the RF system's longitudinal restoring force, effectively the width and centroid of the RF bucket will be modulated in time. If this modulation frequency is close to the synchrotron oscillation frequency, then the centroid of an unexcited bunch can be driven to a large amplitude. This will produce a distribution of particles whose centroid is displaced significantly (in terms of the RF bucket) from its equilibrium location. In fig. 2(b), we see that for particles with large amplitudes, since the phase potential $V(\tau)$ is stronger than a parabolic potential at large amplitude (due to the cosine function), the phase space trajectories tend to crowd closer together for large excursions in τ. This compression of phase space trajectories produces a modulation in the observed symmetry of the temporal distribution of a bunch executing large amplitude oscillations. This asymmetry should be most visible at the largest excursions of the centroid in τ. A pictorial representation, ignoring potential well distortion, of the dynamics in

longitudinal phase space is given in fig. 3. The asymmetric distributions displayed in fig. 3(b) are determined from equation 3. The convention of the asymmetric distribution is as follows: (i) when the asymmetry factor is negative the front (head) of the distribution is shorter and the back (tail) of the distribution is longer. (ii) A positive asymmetry factor has a longer head and shorter head. (iii) When the asymmetry factor is zero, the distribution is a normal Gaussian distribution.

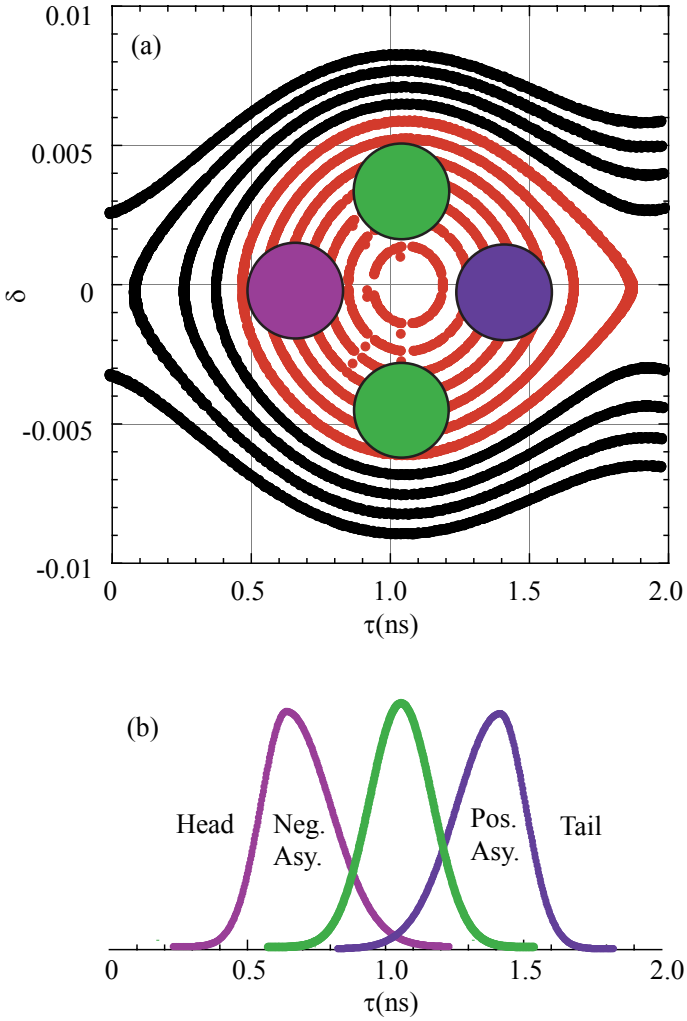

FIG. 3 (color). (a) A bunch experiencing a large amplitude oscillation in longitudinal phase space. (b) A temporal projection of the bunch at three different displacements in longitudinal phase space. The temporal bunch distribution is symmetric or asymmetric depending on its position in longitudinal phase space.

(b) Multiple Bunch Longitudinal Dynamics

The configuration of multiple bunches in CESR is shown in fig. 1. At low current (below the instability threshold) the longitudinal dynamics of all the bunches is similar to single bunch dynamics. As the current increases the instability appears. The instability has been identified as a longitudinal dipole-coupled bunch instability, which is only observed with multiple bunches per train. The detailed characteristics of the instability are described elsewhere [4]. The threshold of the instability

depends upon the bunch spacing. We observed that: 1) at the instability threshold current for some value of n, a signal at $nf_r \pm f_s$ appears in the beams spectra, which indicates a predominately dipole motion in phase space. 2) The threshold current for the instability is dependent on the bunch spacing in the train. 3) The instability reduces the CESR high-energy physics luminosity. 4) When the normal conducting RF cavities were present in CESR, as the current is increased well above the instability threshold a signal at $mf_r \pm 2f_s$ appears, for some value of m[2]. This higher mode of the bunch's oscillation has not been observed with the superconducting cavities up to 350mA for a single beam.

High intensity bunches act as sources of electromagnetic fields called wakefields, which react back on the bunches in the storage ring. The wakefields can be modified by changing the vacuum chamber of the storage ring. Such a change has occurred with the installation of superconducting RF cavities. The wakefields can result in an oscillation in longitudinal phase space trajectories, a change in the bunch distribution, or can cause an instability. The longitudinal dipole-coupled bunch instability is observed in CESR as the collective motion of all the bunches. A detailed theoretical description is outside of the scope of this paper[5]. The dipole-mode corresponds to the rigid motion of the centroid of the bunch about the low current equilibrium point in longitudinal phase space. Figure 4 gives two possible unstable modes of oscillation. If the attenuation of the wakefield is weak in comparison to bunch spacing, then adjacent bunches, and even adjacent trains, will affect each other. If the attenuation is strong, then the bunches ignore each other.

The wakefields that couple from bunch to bunch are like the V_{ext}, described previously, that drives the bunches to large amplitudes in their RF buckets. Consequently, we would expect large amplitude oscillations driven by the wakefields to change the bunch distribution, as shown in fig. 3(b). This change in bunch distribution has been measured in CESR as a change in the bunch asymmetry and is discussed later in this paper.

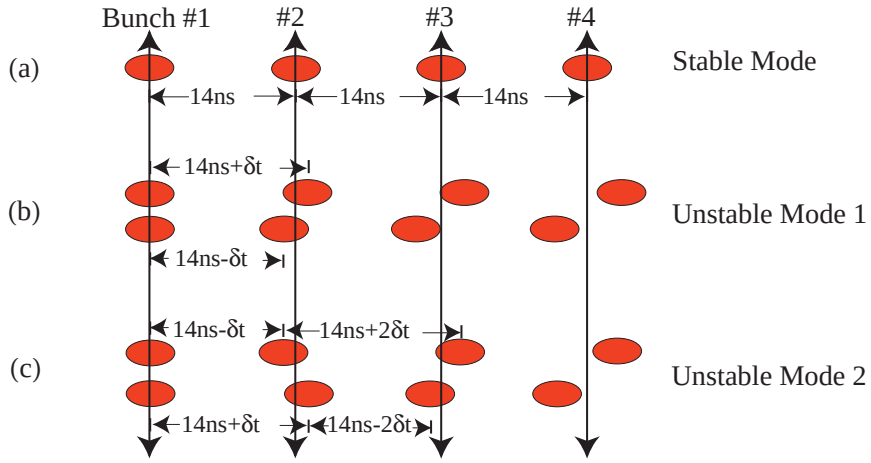

FIG. 4 (color). A description of the dipole-modes of oscillation is made with this diagram. If the bunches are stable and arrive at 14ns intervals they are depicted in (a). Two possible unstable modes of oscillation are depicted in (b) and (c).

The rigid centroid motion of bunches due to the LDCBI has another consequence. The time oscillation of the bunches degrades the luminosity in CESR. The luminosity of an electron-positron storage ring is

$$L \approx \frac{f_0 N \gamma \xi}{2 r_e \beta_V^*}$$

where N is the number of particles per bunch, f_0 is the revolution frequency, r_e is the classical electron radius, ξ is the beam-beam parameter, $\gamma = E/mc^2$, and β_V^* is the vertical beta function at the interaction point. The luminosity is inversely proportional to the vertical beta function and we will try to correlate the decrease in the betatron function, and hence luminosity, due to the dipole mode LDCBI. This factor can be determined from the oscillation of the bunches at the interaction point. The betatron function at the interaction point varies like

$$\beta_v(s) = \beta_v^* + \frac{s^2}{\beta_v^*}$$

where s is the location from the center pint of the interaction point and β_v^* is the interaction point betatron function which happens to be 1.8cm during this experiment. S. Milton calculated the effect of bunch length on luminosity (the "hourglass effect") for the present conditions, but with head on collisions rather than angle collisions[6]. He defines the suppression factor S_f, which is the unitless factor multiplying the short bunch length luminosity L_0, as

$$L_0 = \frac{N^2 f_0}{4\pi\sigma_x\sigma_y}$$

where σ_x, σ_y are the beams transverse sizes at the interaction point, to give the luminosity as a function of bunch length

$$L = L_0 S_f\left(\sigma_z, \beta_v^*\right).$$

For the present case of $\beta_v^* = \sigma_z = 18\text{mm}$, results in $S_f = 0.81$. The ratio of luminosity when the beams are unstable/stable is given by

$$\frac{L_u}{L_s} = \frac{S_f(\sigma_z)_u}{S_f(\sigma_z)_s}$$

where u-subscripted terms are in unstable conditions and the s-subscripted terms are in stable conditions. A measurement of the degradation of luminosity is presented later in the paper.

III. Streak Camera

The characteristics of the longitudinal dipole-coupled bunch instability was measured using synchrotron light from either the electron or positron bunches and a dual sweep synchroscan streak camera (DSSSC). The synchrotron light is emitted from the bunch as it travels through a dipole magnet vacuum chamber. The light is extracted and transported from the vacuum chamber to the streak camera by a series of mirrors. These mirrors transport the light over a path of 17m to the streak camera.

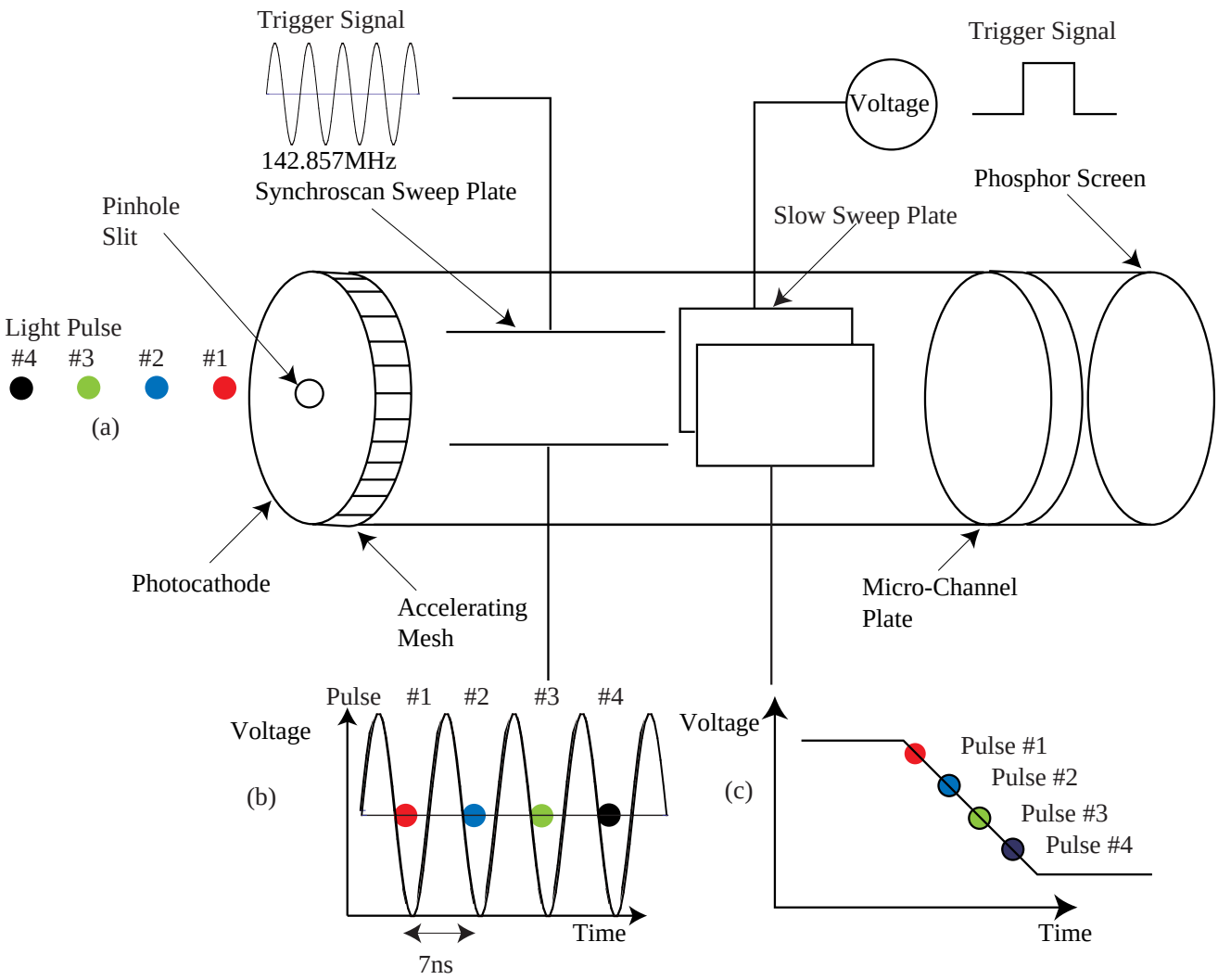

FIG. 5 (color). (a) The four pulses that enter the streak camera are separated in time. (b) The four photoelectrons arriving on the zero crossing of the oscillating voltage. (c) The four pulses arriving on the slow sweep voltage where each photoelectron is deflected at a different angle dependent on its arrival time.

To understand the operation of the DSSSC, fig. 5 depicts the major components of the camera. The workings of the DSSSC can be described in the following manner: consider four pulses of light that are separated in time as they enter the streak camera (fig. 5(a)). These four pulses can be tracked through the camera to illustrate its basic operations. The four pulses enter the streak camera through a pinhole slit that has, typically, a 50μm diameter. The pulses are transported through the streak camera input optics which form an image of the pinhole slit onto a photocathode. The pulses hit the photocathode of the streak tube where they are converted into photoelectrons. The number of photoelectrons produced is proportional to the number of the photons in the input pulse. The photoelectron pulses are again spaced by their arrival time. The emitted photoelectron pulses are accelerated by an accelerating mesh, which pulls the photoelectrons away from the photocathode and

keeps the pulses separated in time. The photoelectron pulses are deflected by two plates, a fast synchroscan sweep plate, and a slow sweep deflection plate. The fast synchroscan plate is triggered by a 142.857MHz timing signal. The frequency of 142.857MHz was chosen to allow the bunches to be on every voltage sweep when the bunch spacing has an integral bunch spacing of 7ns. In routine operation of CESR bunches are spaced every 14ns. The sweep for the fast plates oscillate and data is acquired on every voltage sweep near the zero crossing (fig. 5(b)). If the slow sweep is turned off, the fast sweep superimposes all bunches within the cameras exposure time. The synchroscan unit alone intensifies weak light pulses by repetitive sweeps over a long exposure time. The slow sweep, which is variable between 100ns to 100ms, sweeps the other plane and separates the four pulses (fig. 5(c)). By sweeping both plates, simultaneous measurement of several pulses of light can occur (fig. 6(a)). After the two deflection plates, the electrons enter the micro-channel plate which multiplies the electron pulse by several thousand times. Then the photoelectrons strike a phosphor screen where they are converted into light again. The brightness of the phosphor screen is proportional to the intensity of the pulse. The vertical axis on the phosphor screen is the fast time axis and the horizontal axis is the slow time axis (fig. 6(a)). The image on the phosphor is transported by the output optics to a cooled CCD camera where the image is then digitized and processed by a computer. Longitudinal profiles of an image are to be analyzed offline.

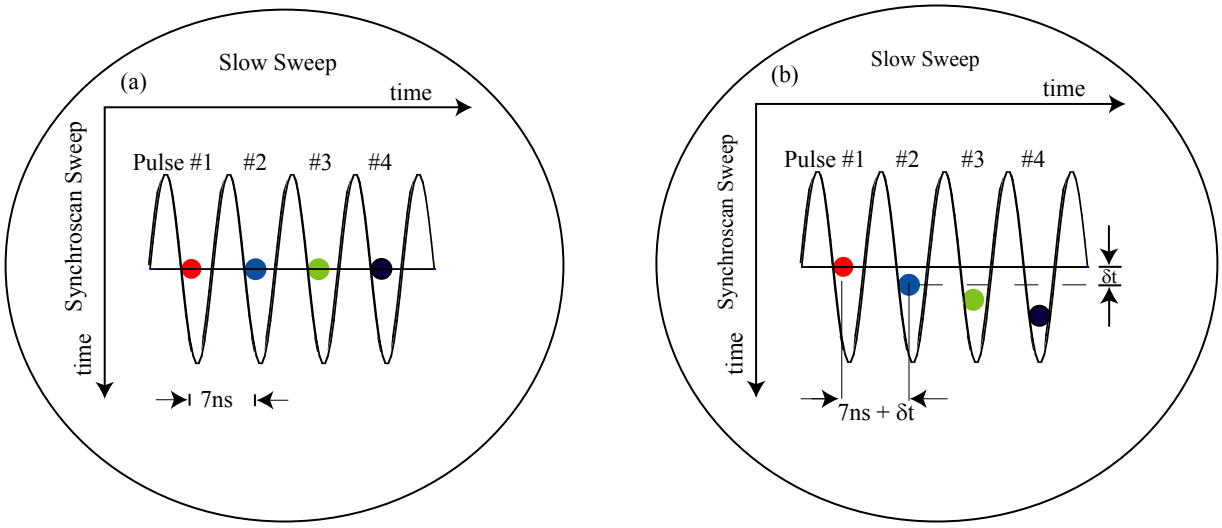

FIG. 6 (color). (a) The four pulses separated by 7ns read-out by the streak camera. (b) The four pulses each separated by 7 + δt ns.

A typical streak camera image is shown in fig. 7. The longitudinal information of each light pulse (trains in this instance) is extracted in the following way. Each pulse is selected with the vertical cursors shown in the fig. 7. Between the vertical cursors, the pixels are summed horizontally to create the longitudinal profile of the bunch distribution (displayed on the left-hand side of the image). For each image, a longitudinal profile for each light pulse is created, saved, and processed off line. The processing includes fitting the longitudinal profile to an asymmetric Gaussian function given by

$$I(z) = I_0 + I_1 \exp\left\{-\frac{1}{2}\left(\frac{(z-\bar{z})}{(1+\mathrm{sgn}(z-\bar{z})A)\sigma}\right)^2\right\} \quad (3)$$

where I_0=pedestal, I_1=peak of the asymmetric Gaussian. The term $\mathrm{sgn}(z-\bar{z})A$ is the asymmetry factor that parameterized the shape of the asymmetric Gaussian.

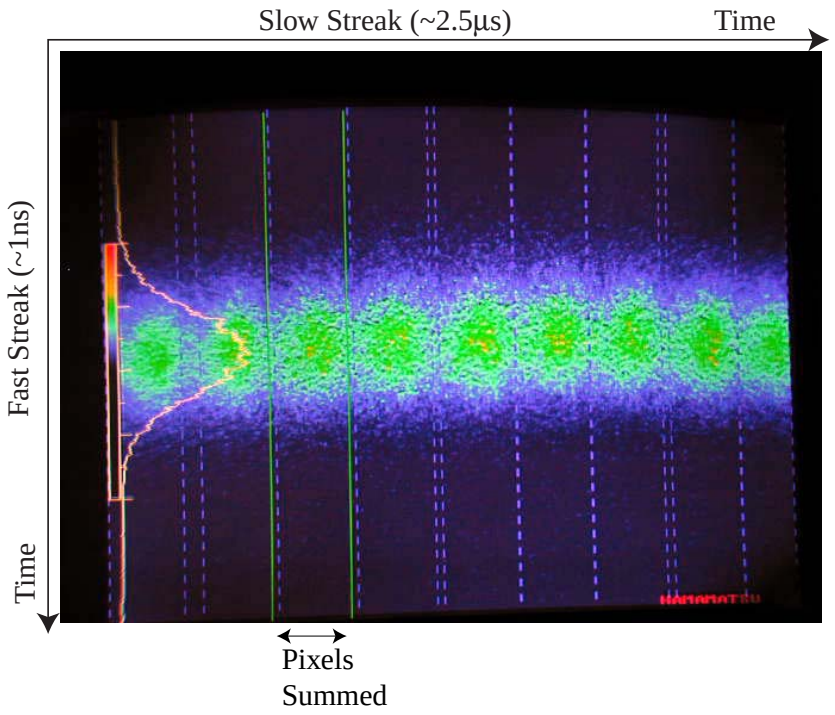

FIG. 7 (color). This is a sample image of nine positron trains in CESR. Taking a vertical slice and summing the pixels between the slices gives the longitudinal profile shown to the left. The green lines denote the vertical slice that is the summed train. The profile of the distribution is displayed to the left. A profile of the train is displayed in figs. 13 where the distributions are fit to a Gaussian function. For this image, nine longitudinal profiles were saved.

With the basic operation of the DSSSC described above, an explanation of the longitudinal dipole-coupled bunch instability as seen by the streak camera is in order. Under normal operation, bunches within a train are separated by 14ns, which would be two sinewaves apart at 142.857MHz. If they deviate from the 14ns spacing, the bunches will have different phases on the sinewave, and this phase difference is detected by the DSSSC. Any instability corresponding to centroid motion in longitudinal phase space can be detected with the DSSSC. An example of a stable and unstable train of bunches is displayed in fig. 6(a) and (b) when the bunches are separated by 7ns.

In order to quantify the systematic errors involved with the streak camera, the linearity of the camera was measured during high-energy collisions in CESR. The measurement consists of taking streak camera images of one train and fitting each bunch in the train to an asymmetric Gaussian function to determine the bunch length and asymmetry factor. Images were taken at different trigger settings to determine the linearity of the streak voltage for the synchroscan unit. The bunch length (in

terms of pixels) as a function of the mean position on the synchroscan timing without the streak camera linearity is plotted fig. 8(a). Without the streak voltage calibration, the bunch length is highly correlated with the synchroscan unit timing. The calibration curve for the synchroscan unit is displayed in fig. 8(b).

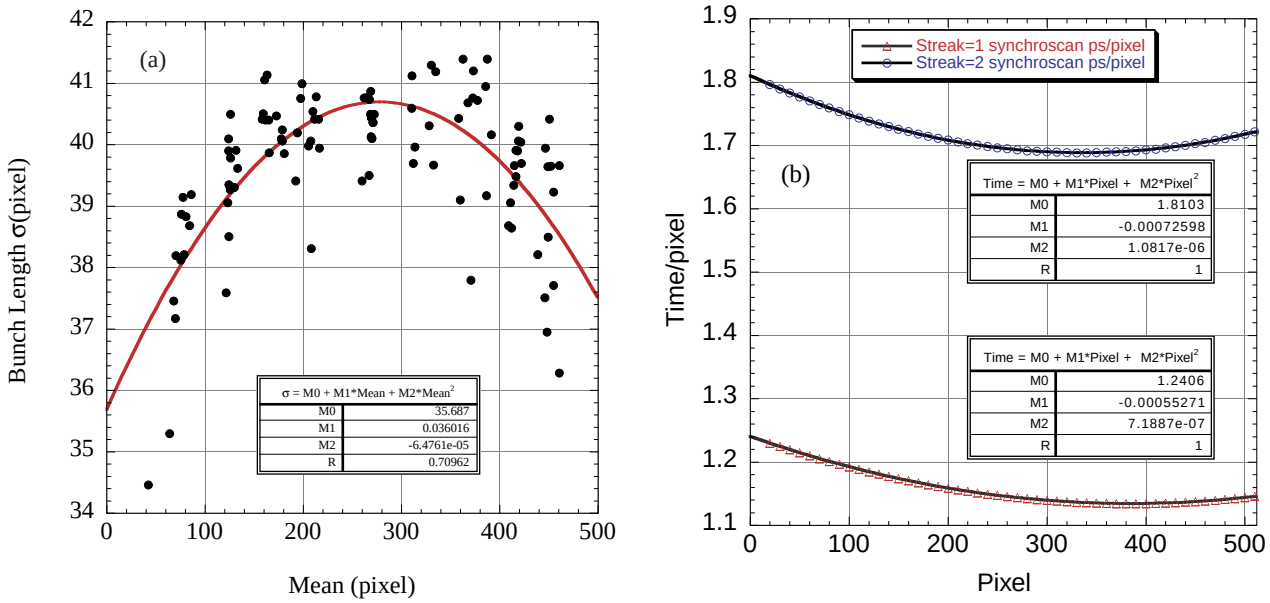

FIG. 8 (color). (a) The measured bunch length at different trigger settings without the calibration correction. (b) The synchroscan unit calibration curve.

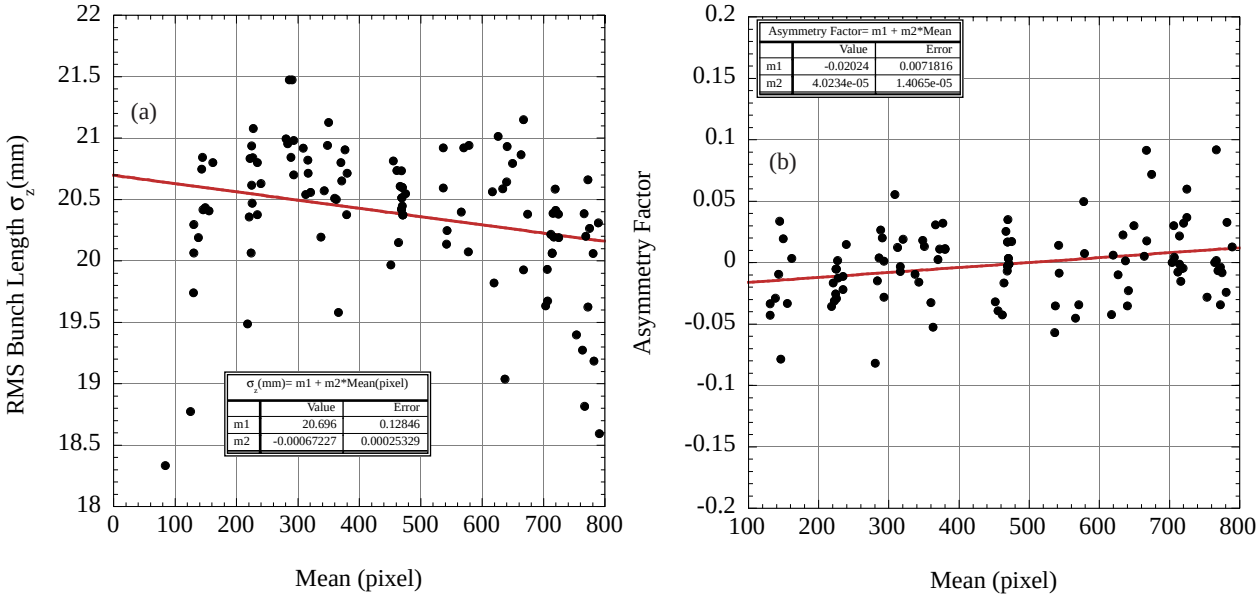

FIG. 9 (color). (a) The bunch length and (b) asymmetry factor as a function of trigger setting using the synchroscan calibration curve shown in fig. 8(b).

Using the calibration curve from fig. 8(b), the calibrated bunch length and asymmetry factor is determined. Figure 9(a) is the bunch length and (b) is the asymmetry factor as a function of synchroscan unit timing. Both the bunch length and asymmetry factors are slightly correlated with

the synchroscan unit timing but the spread in the data is due to statistics and current fluctuations. The bunch length for the different bunches in the train is displayed in fig. 10. Two comments can be made about the data. 1) The bunch length for the last bunch in the train is smaller than the other three. This is due partly to the lifetime in bunch four being lower that results in a lower bunch current for the fourth bunch at the time of the scan. This can explain partly the large differences in the bunch length and asymmetry factor compared to the other bunches. 2) There are large fluctuations in the bunch length when the timing is at either extreme of the synchroscan timing. Measurements taken in this paper are with the image towards the center of the streak sweep timing.

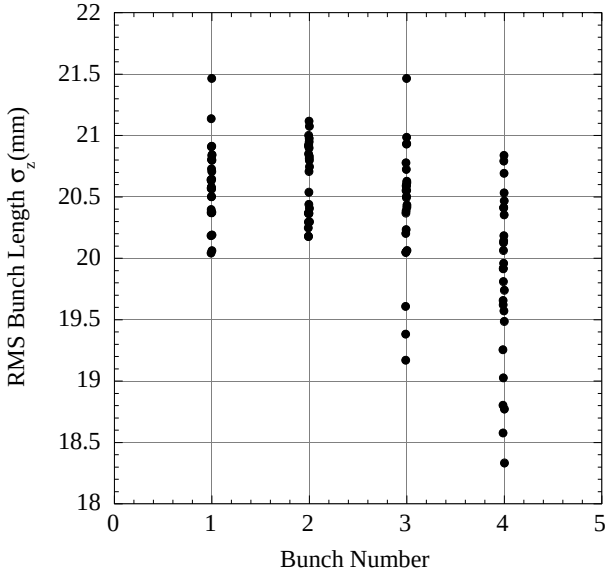

FIG. 10. The bunch length for the four bunches in the train. The mean bunch length for bunch 1 through 4 are 20.6± 0.3mm, 20.7± 0.3mm, 20.4± 0.5mm, and 19.8± 0.7mm respectively.

IV. Measurement of the Longitudinal Dipole-Coupled Bunch Instability

The following experiments were performed with the dual sweep streak camera: A) Measurement of a single train consisting of four bunches with the longitudinal dipole-coupled bunch instability present. B) Measurement of multiple trains with the instability present. C) Oscillation of bunches during collisions to quantify the luminosity degradation due to the instability. Above the instability threshold the LDCBI is present, except when the longitudinal feedback system is turned on. During normal operation, the feedback system must remain on. The following experiments were performed during special machine studies times when the feedback system could be turned off to induce the instability.

A. Single Train Measurements

With positrons present in CESR, single train measurements of the longitudinal dipole-coupled bunch instability were performed. Setting the slow streak speed to a full sweep range of 100ns allows

the single train dynamics to be measured. The measurements were made with nine trains of positrons, with four bunches per train, present in CESR. The bunch spacing in each train was 14ns. At this bunch spacing, the instability threshold is approximately 180mA total or 5mA per bunch. Measurements were made at total beam current between 180mA and 350mA.

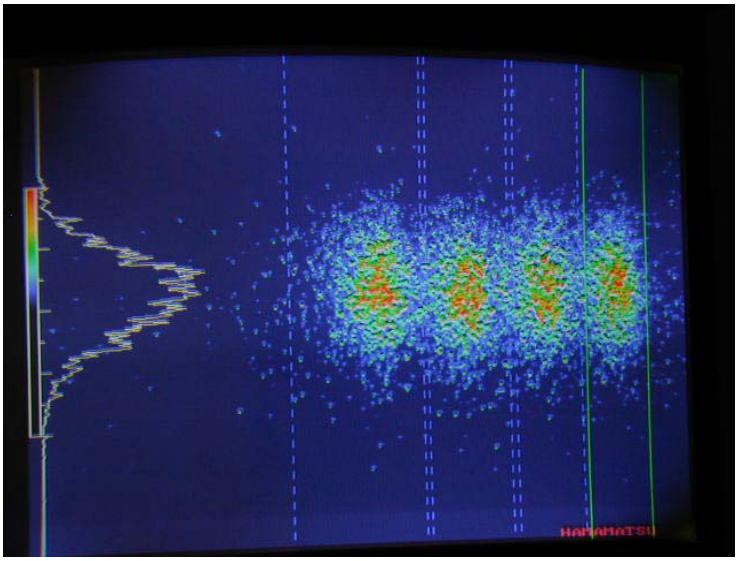

FIG. 11 (color). A typical streak camera image of a stable train of positron bunches when the longitudinal feedback is turned on.

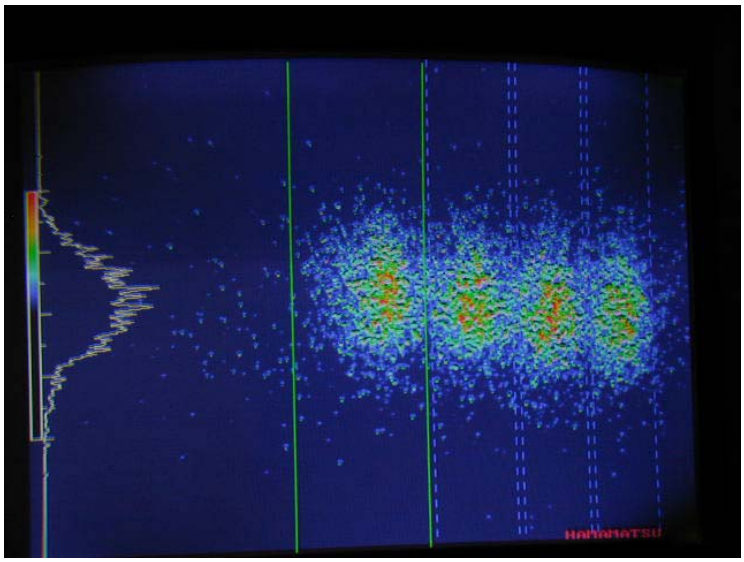

FIG. 12 (color). A typical streak camera image of a single train of bunches in CESR with the longitudinal feedback turned off and the LDCBI present

The presence of the LDCBI was determined by two methods: 1) above the instability threshold with longitudinal feedback turned off, a signal indicating a dipole instability is observed using a spectrum analyzer. The signature of the instability is synchrotron sidebands clearly visible at $f=nf_r \pm f_s$. During this experiment, a spectrum analyzer was used to measure the amplitude and frequency of the beam spectra for $f=f_r+f_s$. The results are listed in table 2. 2) The dual-sweep streak camera can detect the LDCBI. Figure 11 and Fig. 12 are images of a single train of bunches without

and with the instability present. When the instability is present, the profiles of the four bunches do not align vertically, as shown in figure 12. The images with the instability present were chosen due to observed large time oscillations.

Current (mA)	fr +fs (kHz)	Amplitude (dBm)
183-181	410.75	-35.3
227-224	410.68	-19.6
276-272	410.60	-18
326-316	410.45	-31.1
350-344	410.38	-28.8

TABLE 2. The measured currents, dipole-mode frequency, and intensity for these measurements.

Several single trains images, like the ones in figs. 11 and 12, were made at different beam currents, with and without the instability present. For each image, the longitudinal profile of each bunch in the train was fit to an asymmetric Gaussian function. The amplitude of time oscillation for each bunch is quantified by computing the shift in its centroid (mean) relative to the other bunches in the train. If the bunches are stable, the centers of the four bunch distributions in a train should superimpose in time. If the longitudinal dipole-coupled bunch instability is present, the bunches centroids oscillate in time, and will not in general be aligned in time. In fig. 13 the longitudinal distributions of bunches in a single train are superimposed for the case when the beam is stable (a) and unstable (b).

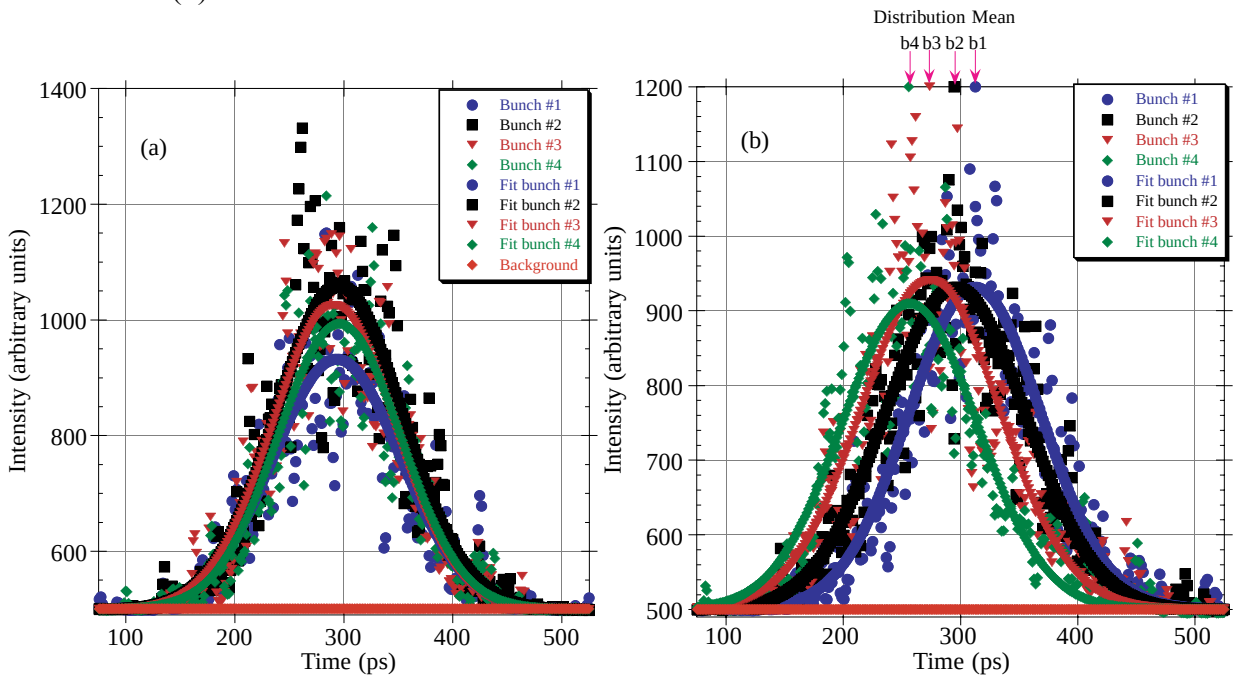

FIG. 13 (color). The four longitudinal profiles from a single image when the dipole mode coupled bunch instability is (a) not present and (b) present. The mean of the individual distributions when the instability is present is shown above (b). The total positron current when these images were taken was 276mA.

A spectrum analyzer was used to determine the strength of the LDCBI in conjunction with the streak camera images. As the total beam current increase the amplitude of the instability increased for the first three measurements (I=183-276mA), and decreased for the last two measurements (I=326-350mA). This drop in amplitude can be attributed to a different mode of oscillation in the bunch train, and will be discussed later.

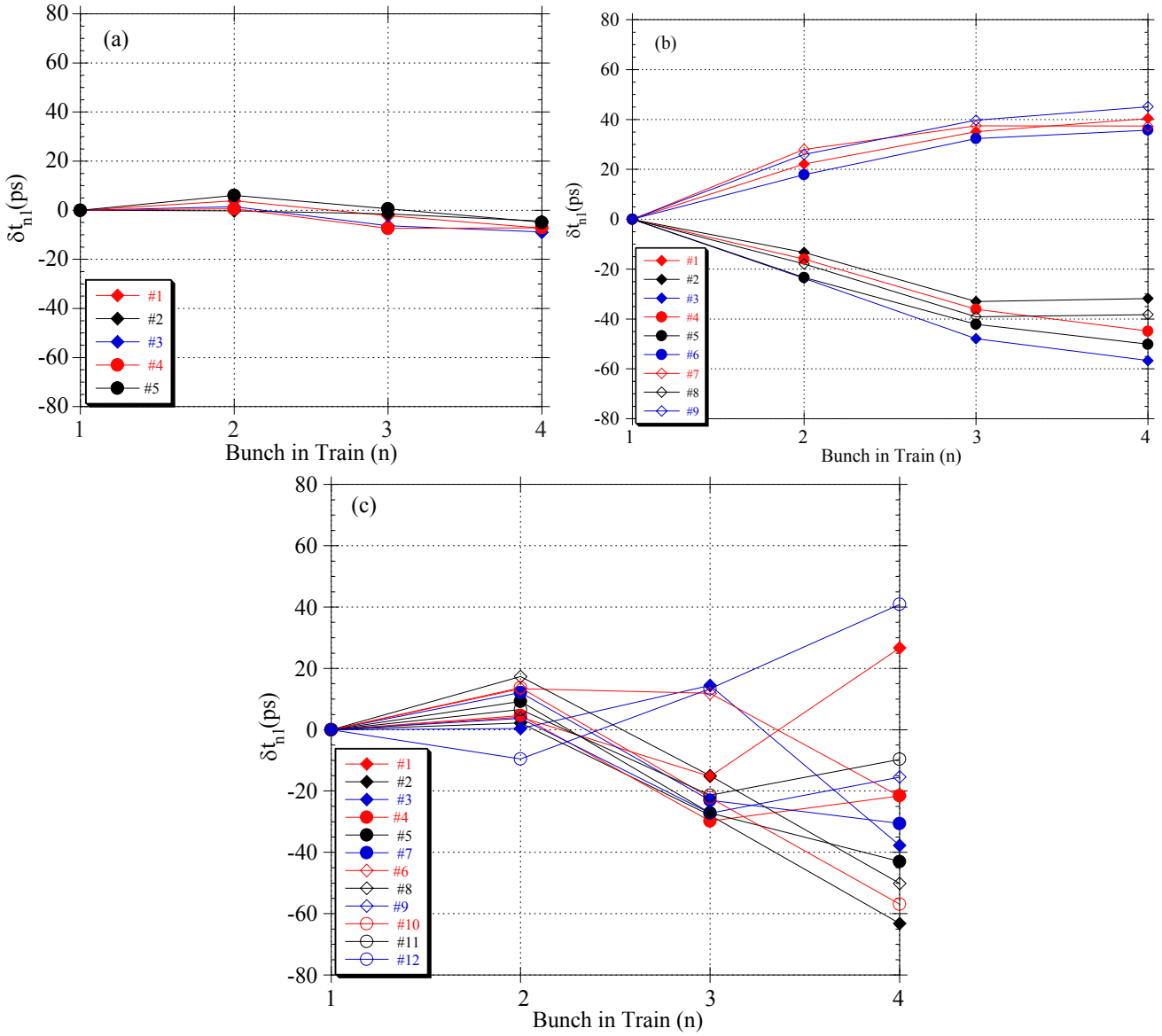

FIG. 14 (color). The time of arrival oscillation (δt_{n1}) when (a) the train is stable and the total beam current is 276mA, (b) the train is unstable and the total beam current is 276mA and (c) the train is unstable and the total beam current is 326mA.

Under stable conditions the bunches in a train are separated by 14ns. When the instability is present, the bunches in a train oscillate about the 14ns spacing. The amplitude of the time oscillation is determined from the longitudinal profiles fit to an asymmetric Gaussian function. The centroid position of the bunch is determined from the fit to the data. For our analysis, the amplitude of the

time oscillation is referenced to the leading bunch (first bunch in the train). The change in arrival time for the bunches after the leading bunch is given by

$$\delta t_{n1} = \text{Mean}_n - \text{Mean}_1 \quad \text{for } n = 2,3,4$$

where n is the trailing bunch number. The sign convention is the following: A positive δt_{n1} means the trailing bunch arrives (n-1)14ns+δt_{n1} later after the leading bunch in a train. The time deviation from the lead bunch is displayed for a number of sample triggers in fig. 14 for each of three different cases: (a) when the train was stable at a current of 276 mA, (b) when the train was unstable at a current of 276 mA, and (c) when the train was unstable at a current of 326mA.

Several comments can be made about the results:

1) Using this analysis technique it is easy to see that the bunches in a train oscillate in time. The longitudinal feedback system stabilizes the bunch time oscillations to a few picoseconds. When turned off, the time oscillation has been measured to approximately 100ps. The unstable time oscillations substantially degrade the High-Energy Physics luminosity.

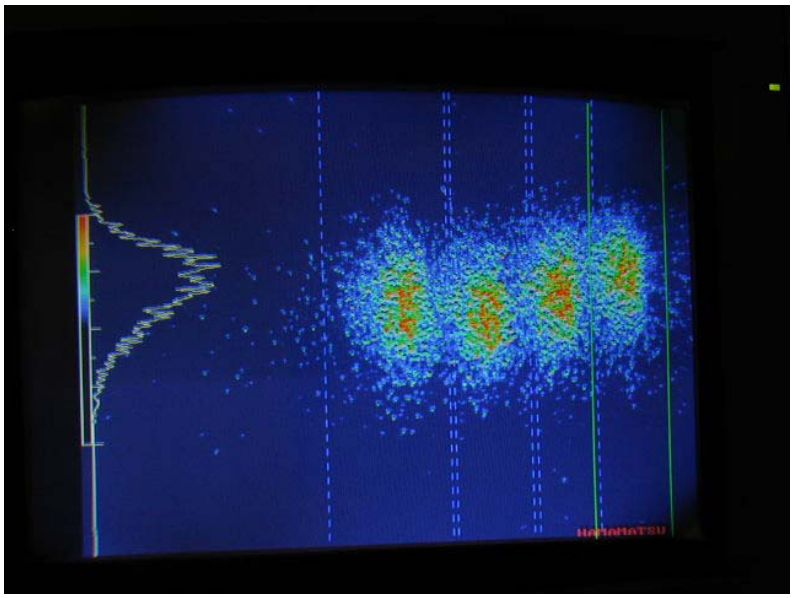

FIG. 15 (color). A typical streak camera image taken with 326mA of positrons present in CESR. The second bunch in the train arrives later than the first bunch. This signifies a change in the instability's oscillation mode.

2) The data suggests a change in bunch oscillation mode occurs between 276mA and 326mA. At 276mA and below, all the bunches move closer, or further away in unison, according to fig. 14(b). This motion, from now on referred to as "accordion" oscillation, is displayed in fig. 4(b) as unstable mode 1, and is detected in the fig. 12 streak camera image. At 326mA and above, the accordion oscillation changes according to fig. 14(c). The second bunch in the train oscillates in the opposite direction as the third and fourth bunch. This mode of oscillation is depicted in fig. 4(c) as unstable mode 2, and is evident in the streak camera image shown in fig. 15. These

measurements, in conjunction with the spectrum analyzer results, reveal that the change in oscillation mode occurs between 276 and 326mA.

3) The dipole mode signal (and no signals indicating higher modes of oscillation) was the only signal observed by the spectrum analyzer during these measurements.

The time deviation of adjacent bunches due to the LDCBI can be defined as

$$T_{mn} = |\text{mean}_m - \text{mean}_n|$$

where mean_m and mean_n are the mean centroid positions of adjacent bunches in the train. The results of this calculation are displayed in fig. 16.

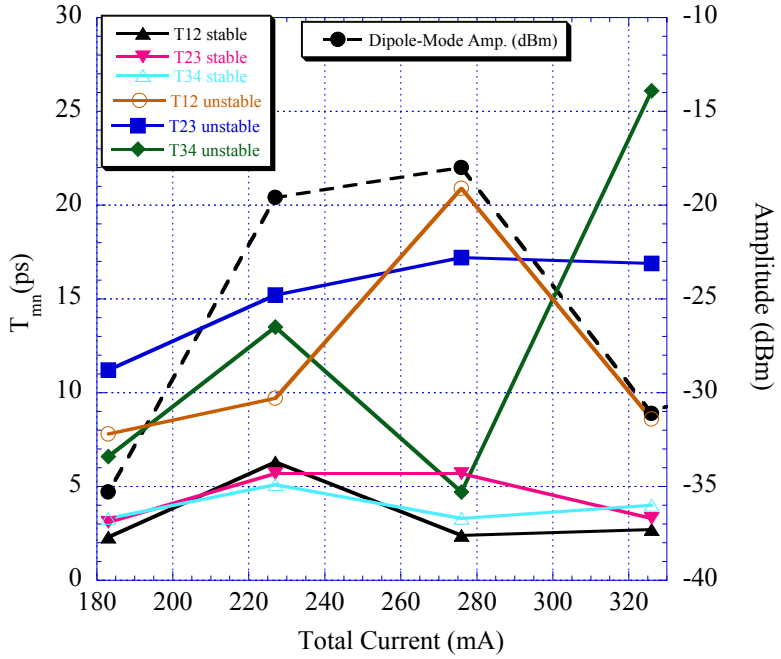

FIG. 16 (color). The time deviation between adjacent bunches in a train as a function of current, with and without the instability present.

The results suggest that:

(i) When the bunches are stable, the deviation between bunches averages 3.4ps for T_{12}, 4.5ps for T_{23}, and 4.0ps for T_{34}. When unstable, the average time deviation is 11.6ps for T_{12}, 19.6ps for T_{23}, and 15.4ps for T_{34} suggesting that the bunches move in synchronous phase relative to one another on the average of 10 to 15 picoseconds over the current range of 180 to 330ma. This might suggest a systematic change in bunch length through each train or some large change in the beams wakefield.

(ii) The average time deviation, between T_{23} and T_{34} increases, and T_{12} decreases, at the two highest currents. This jump is another signature of a change in the character of the LDCBI oscillation mode.

When only normal conducting copper cavities were present in CESR, oscillations having the same spectral characteristics as longitudinal quadrupole-coupled bunch oscillations were detected by driving the dipole-mode to high amplitude[2]. The presence of these quadrupole-mode-like oscillations drastically changes the bunch distribution and leads to beam loss. With only the dipole oscillations present, no change in the bunch distribution is expected other than potential well distortion. Potential well distortion, which in CESR changes the asymmetry of the bunch distribution by making the tail longer than the head of the distribution, has been measured on single bunches at CESR[7].

The bunch distribution, as pointed out earlier, does change at large amplitude oscillations. The larger the time deviation behind the first bunch in the train, the larger the asymmetry factor deviates from the head bunch asymmetry factor. This implies that as the time deviation amplitude grows, the bunch asymmetry factor grows. This statement can be verified by correlating the time deviation with the asymmetry deviation. The difference in asymmetry factor between the first bunch in the train and subsequent bunches given by

$$\delta A_{n1} = A_n - A_1 \quad \text{for } n = 2,3,4$$

where A_n is the asymmetry factor for the trailing bunch n. By taking the difference in asymmetry factor between bunches the affect of potential well distortion can be ignored. The time difference between mean positions between the first bunch and subsequent bunches in the train, given by

$$\delta t_{n1} = \text{Mean}_n - \text{Mean}_1 \quad \text{for } n = 2,3,4$$

where n is the trailing bunch number. The correlation between the time deviation and the difference in asymmetry factor is seen in fig. 17.

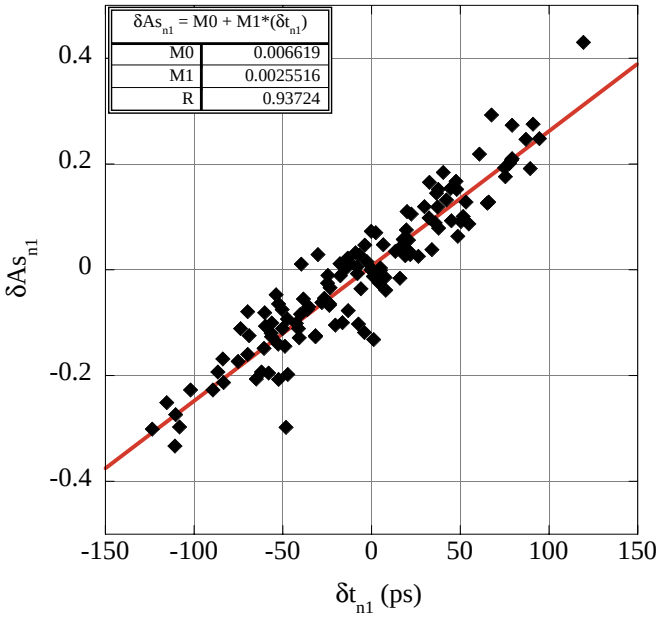

FIG. 17 (color). A plot of the change in the asymmetry factor from bunch one to bunch n as a function of time deviation from bunches one to bunch n. The correlation between these two quantities suggest the change in bunch shape is due to oscillations in the potential well that shapes the bunch distribution.

These two quantities are highly correlated and the following conclusions are made:

1) If the bunches are spaced by 14ns, they are called synchronous and they line up on the vertical axis of the streak camera images. When bunches are unstable, the bunches trailing the lead bunch oscillate about this synchronous location (fig. 6(b)). This oscillation changes the bunch asymmetry factor, as described earlier. If the oscillating bunch arrives early, the tail of the bunch grows, if it arrives late, the head of the bunch grows. Figure 18 (a) and (b) are typical measured bunch distributions that have large time deviations and therefore large asymmetry factors.

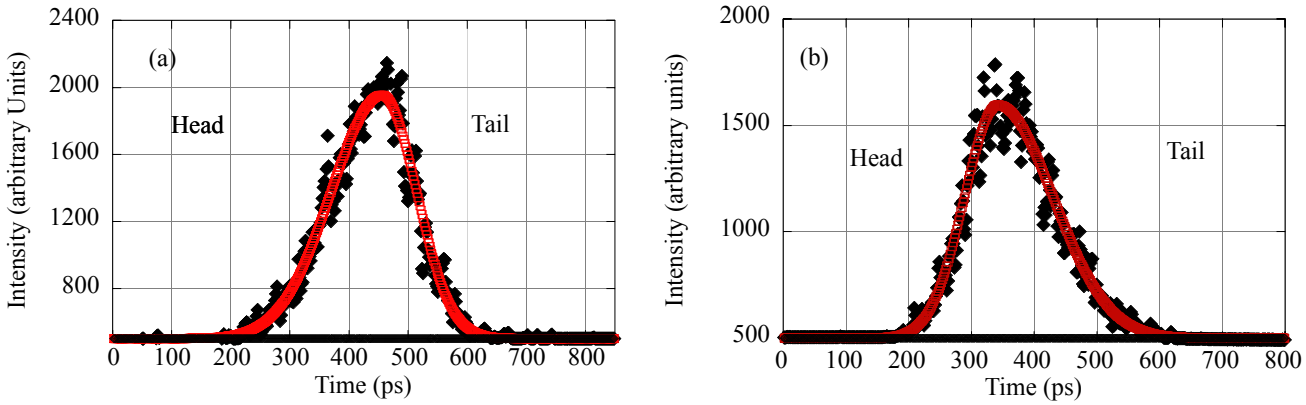

FIG. 18 (color). Two single streak camera distributions fit to an asymmetric Gaussian function where the asymmetry factor and time deviation between bunches is (a) $\delta As_{31} = 0.2$ and $\delta t_{31} = 79ps$, (b) $\delta As_{41} = -0.23$ and $\delta t_{41} = -102ps$.

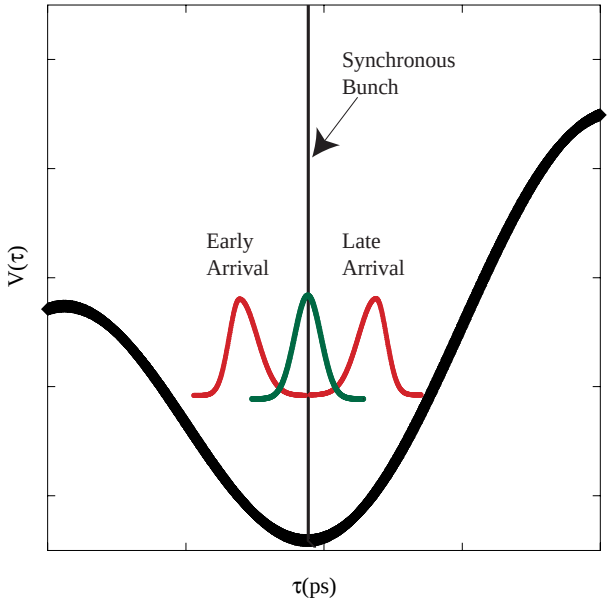

FIG. 19 (color). This figure displays the change in asymmetry of the bunch distribution in its potential well. The larger the time deviations from a synchronous bunch the larger the change in the asymmetry factor.

2) Figure 19 displays the shape oscillation present with a large oscillation amplitude. The asymmetry change is a result of the bunch oscillating in its potential well. A synchronous bunch arrives centered in time with the potential well minimum giving a Gaussian bunch distribution (ignoring potential well distortion). Bunches not centered at the potential well minimum will experience nonlinear forces that change the bunch distribution.

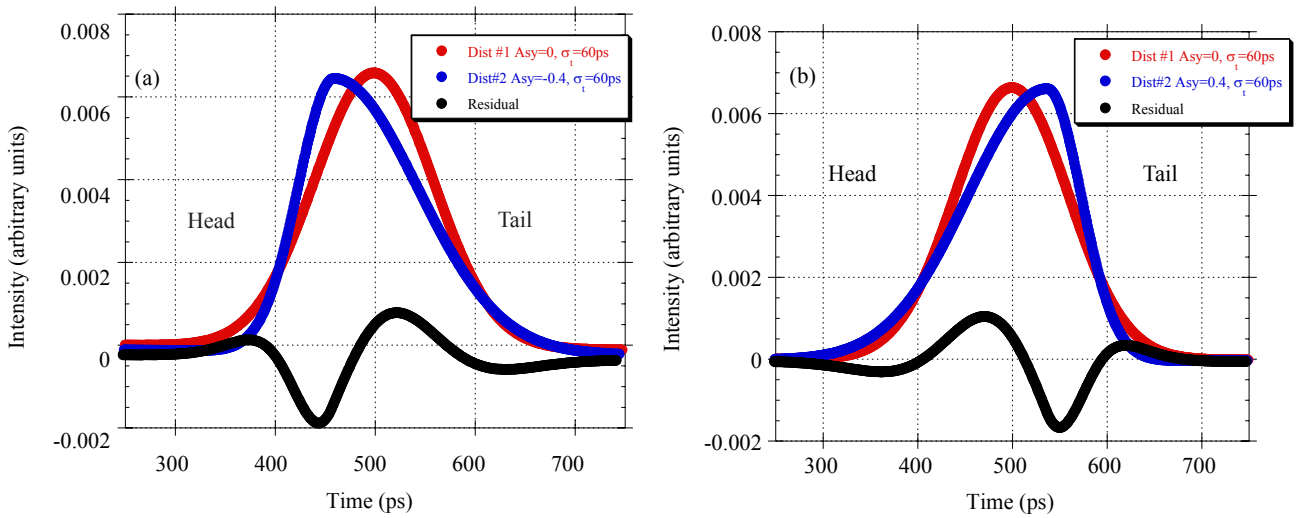

FIG. 20 (color). Two asymmetric Gaussian distributions with the same bunch length and asymmetry factors of (a) A_1=0 and A_2=-0.4, and (b) A_1=0 and A_2=0.4. The residual between the two distributions is also displayed.

3) The correlation between the change in asymmetry factor and time deviation between the lead and trailing bunch, shown in fig. 17, is evidence of charge flow within the bunch distribution. To calculate the amount of charge flow, consider a pure Gaussian distribution (asymmetry factor=0), which has an equal amount of charge in the head and tail of the distribution. If the distribution is suddenly changed, from a pure Gaussian to an asymmetric Gaussian distribution, a flow of charge occurs within the distribution. By superimposing two normalized asymmetric Gaussian distributions with different asymmetry factors, the residual between distributions is determined. Figure 20 (a) and (b) are examples of two superimposed distributions. The charge flow, between the head and tail, with different asymmetry factors is determined by summing the residual in the head and tail of the distribution. A summary of the calculation is shown in fig. 21 (a). The percent of charge flow, as a function of time deviation, is calculated using fig. 17 and 21 (a) and is plotted in fig. 21 (b).

As an example, if a bunch in a train has a $\tau = \pm 100$ps time deviation from the lead bunch, which corresponds to a change in the asymmetry factor of +0.26 (100ps) and -0.25 (-100ps), the flow of charge between the head and tail is approximately 3%. Figure 22 (a) and (b) are the change in distribution (assuming the lead bunch is Gaussian) for a +/-100ps oscillation.

The following conclusions can be made from the above analysis: (i) Trailing bunches in a train oscillates in time behind the lead bunch due to the dipole instability. This time

oscillation leads to charge flow between the head and tail of the trailing bunch distribution. This charge flow occurs at synchrotron frequency. (ii) The amount of charge that oscillates back and forth depends upon the amplitude of time deviation from the lead bunch. The bunch distribution changes shape as a result of this charge flow. This change in the distribution's shape at large dipole oscillation amplitudes may explain the fact that the oscillation amplitude limits, since this affects the way that the self-fields react back on the bunch.

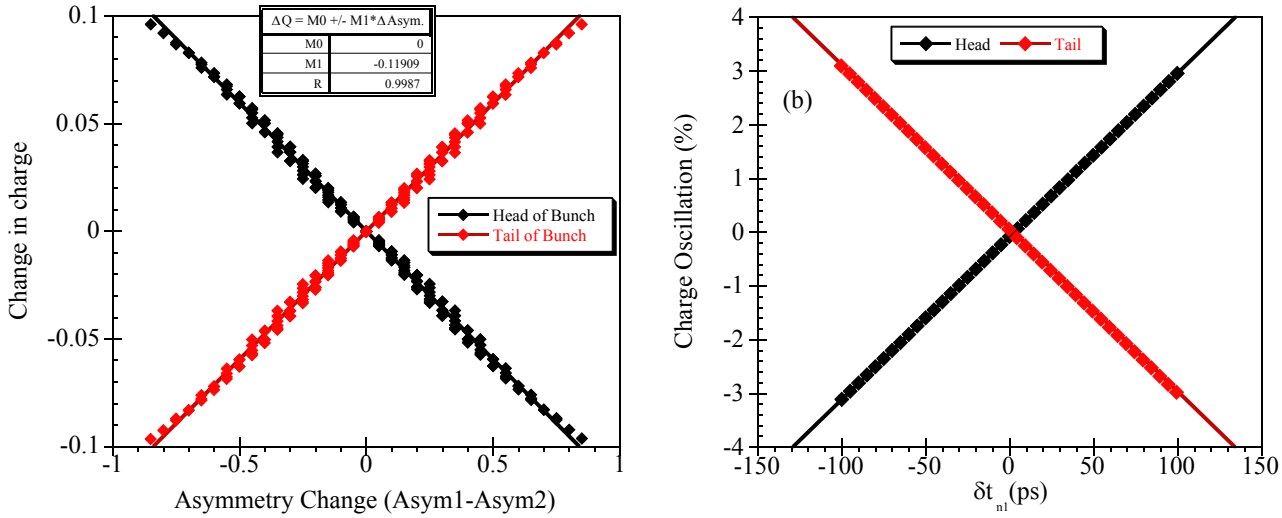

FIG. 21 (color). (a) The flow of charge due to an asymmetry factor deviation between two distributions. (b) The percent of charge flow in a distribution due to a time oscillation from the lead bunch in a train.

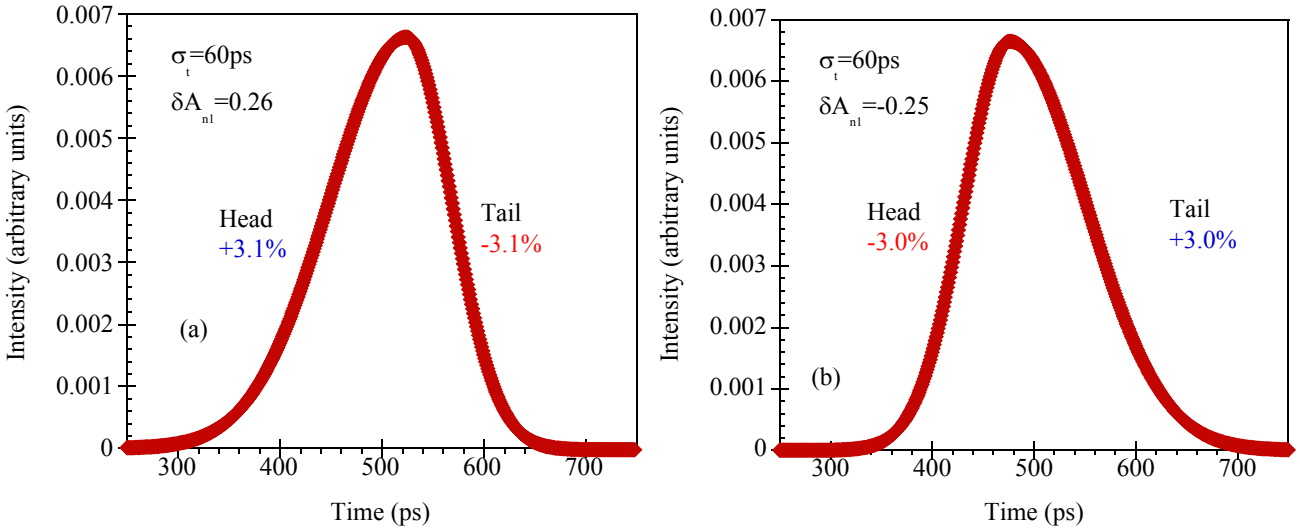

FIG. 22 (color). The change in the trailing bunches in a train (from a Gaussian distribution) due to a (a) 100ps deviation and (b) –100ps deviation from the lead bunch in the train.

The effect of the longitudinal temporal displacements between colliding electron and positron bunches on luminosity may be estimated for head on collisions (rather than angle collisions) from Milton's geometric luminosity suppression factor, S_f, using the present values of β_y^* and bunch length[6]. Extrapolating (slightly) a fit to his calculation to include the value of S_f when the bunch missed colliding in time by one sigma (18mm or 60ps) gives a value of 0.61 for S_f. By comparison bunches colliding in time have a value of S_f of 0.81. Therefore, a one-sigma oscillation of the collision time of bunches yields a geometric reduction of luminosity of 0.75. In addition to the geometric effects, one would expect the appearance of additional beam-beam dynamical effects that would further reduce the luminosity and the lifetime. The presence of large oscillation amplitudes in fig. 17 is suggestive of a very significant reduction in luminosity.

The longitudinal profiles for the four bunches in a train are summed to provide a profile of the train. Each train profile is fit to the asymmetric Gaussian function. The average time deviation, which is the average time the three trailing bunches deviate from the leading bunch, is computed. An interesting correlation can be made (fig. 23). If all the bunches arrive early, the train has a long tail, and a long head for late arriving trains. Figure 24 is a schematic description of the longitudinal dynamics measured. A negative time deviation is early arrival. A train with a negative asymmetry (long tail) and positive asymmetry is shown in fig. 24. A more detailed study of the dynamics in a train will follow in the next section.

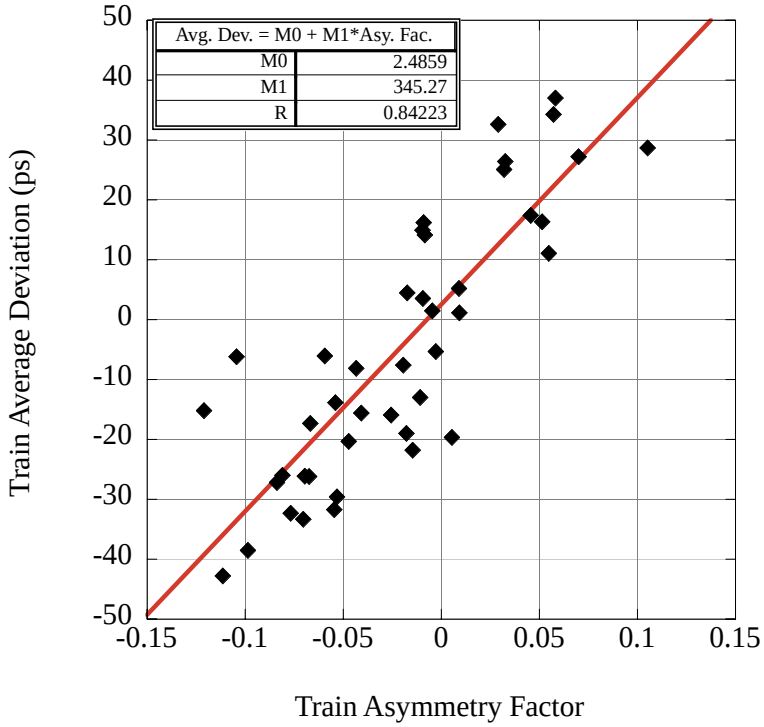

FIG. 23 (color). A correlation between the train asymmetry factor and the average time deviation.

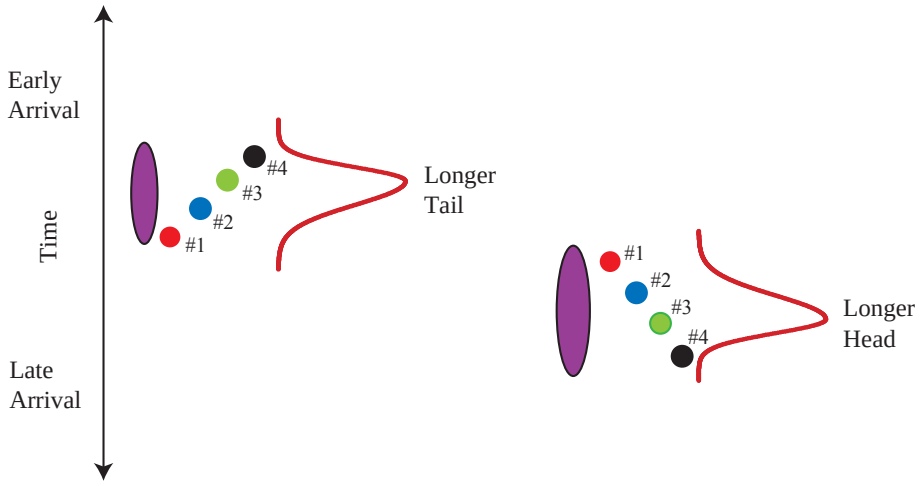

FIG. 24 (color). This figure displays the dynamics of the bunches in a train. A positive time deviation means the bunches in a train arrive late and the train bunch distribution has a longer head. The mode of oscillation is described for current between 183-276mA when the oscillation mode is the accordion oscillation.

B. Multiple Train Measurements

So far, we have concentrated on bunch motion within a single train, and have ignored train to train dynamics. By reducing the speed of the slow streak plane, multiple trains can be observed, with the limitation that bunches within the train cannot be resolved. The measurements presented in this section of multiple trains were made with positrons present in CESR. Figures 25 and 26 show typical images taken with the dual sweep streak camera when nine trains of four bunches per train present in CESR under both stable and unstable conditions. Each train pulse shown in these figures consist of four bunches, and the mean of the train will be referred to as the centroid of the train of four bunches.

As was shown in the previous section, bunches within a train oscillate in time when the longitudinal dipole-coupled bunch instability is present, and it is evident from these images (figs. 25 and 26) the train centroids also oscillate with the instability present. These two separate modes can be classified as bunch modes and train modes[8]. From these images the amplitude of time oscillation for each train was determined by fitting each train profile to an asymmetric Gaussian function. The longitudinal centroid of each train is determined from the fit to the data. For each image, which consists of nine trains, the image centroid, and standard deviation are calculated. If an oscillation is present, the standard deviation will have a component due to bunch length and another component proportional to the dipole oscillation amplitude. For sinusoidal oscillation of the bunch's arrival time the total standard deviation σ_t over many observations will be given by

$$\sigma_t^2 = \sigma_b^2 + \frac{1}{2}\hat{z}^2$$

where σ_b is the bunch length and $\hat{z}$ is the longitudinal spatial oscillation amplitude.

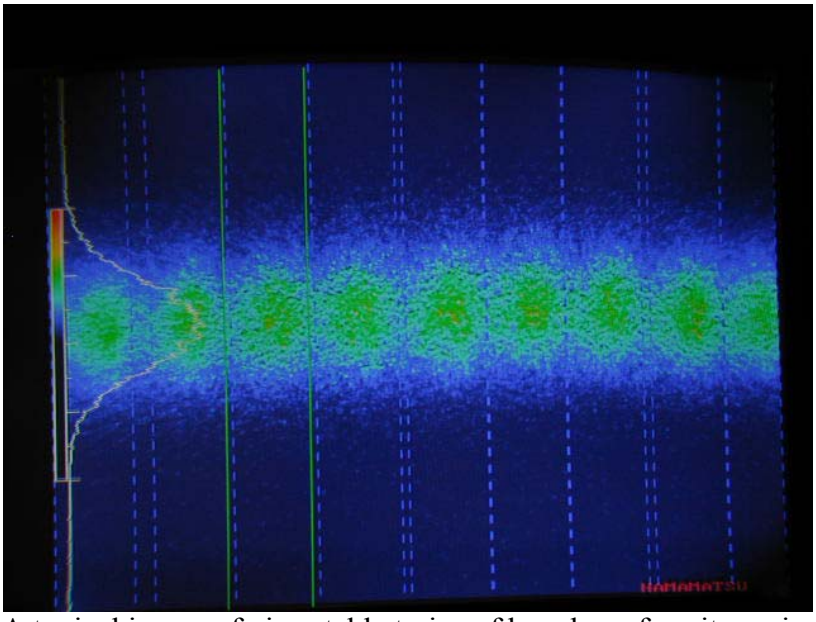

FIG. 25 (color). A typical image of nine stable trains of bunches of positrons in CESR. The total beam current for this measurement was 184mA.

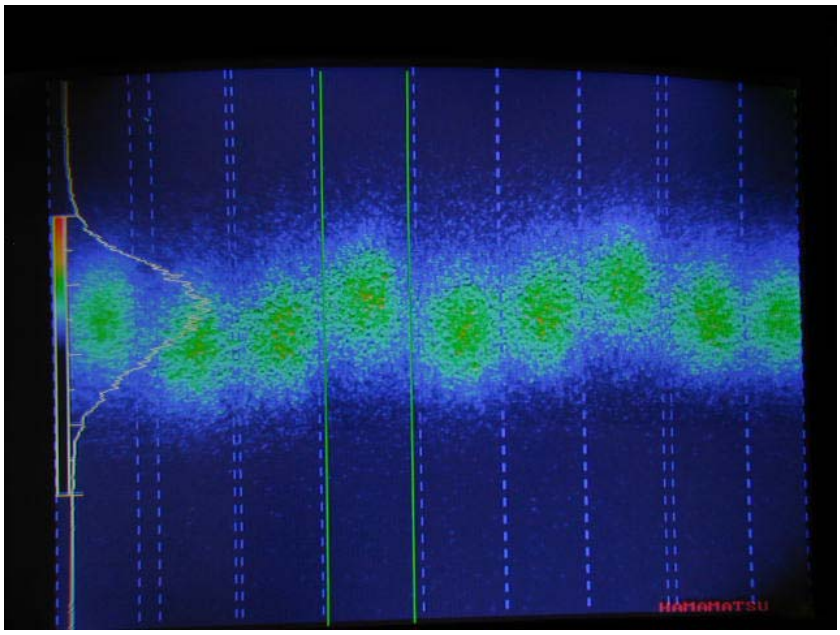

FIG. 26 (color). A typical image of nine unstable bunches of positrons in CESR. The total beam current for this measurement was 184mA.

Figure 27 (a) is a typical train profile fit to an asymmetric Gaussian function. Figure 27 (b) is the mean of the standard deviation of trains distributions at each current with and without the instability present.

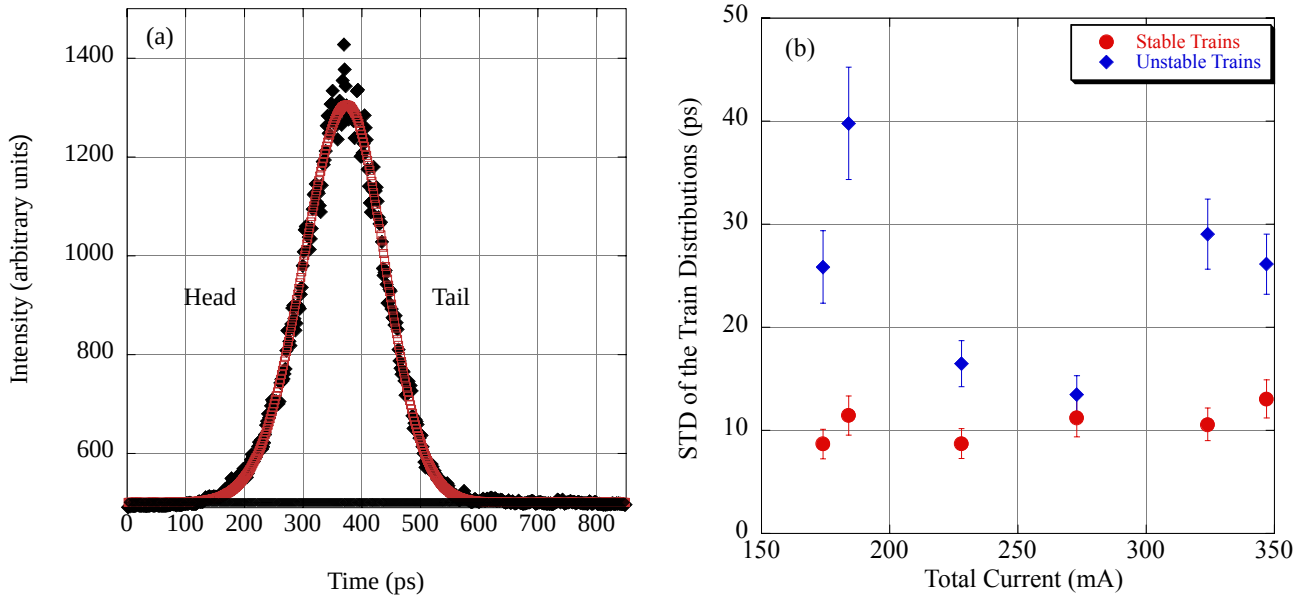

FIG. 27 (color). (a) A typical longitudinal profile of a train fit to an asymmetric Gaussian function. (b) At each beam current, the standard deviation train oscillation was determined with stable and unstable trains.

Several comments can be made about these results:

(i) The standard deviation of the train's distribution's centroid time position is consistently around 10ps when the trains are stable. During unstable operation, the standard deviation increases by up to a factor of four depending on the amount of current in CESR which implies that bunches may have oscillation amplitudes up to 40ps.

(ii) Figures 28 (a)-(c) is the measured centroid under three different conditions, a stable beam, an unstable beam at low current and an unstable beam at high current. For the unstable low current case (b), all the trains correlate in phase with a period three train oscillation but they have slightly different amplitudes. For the unstable high current case (c), there appear period 1 and 1.25 oscillations suggesting the presence of more than a single unstable mode of oscillation.

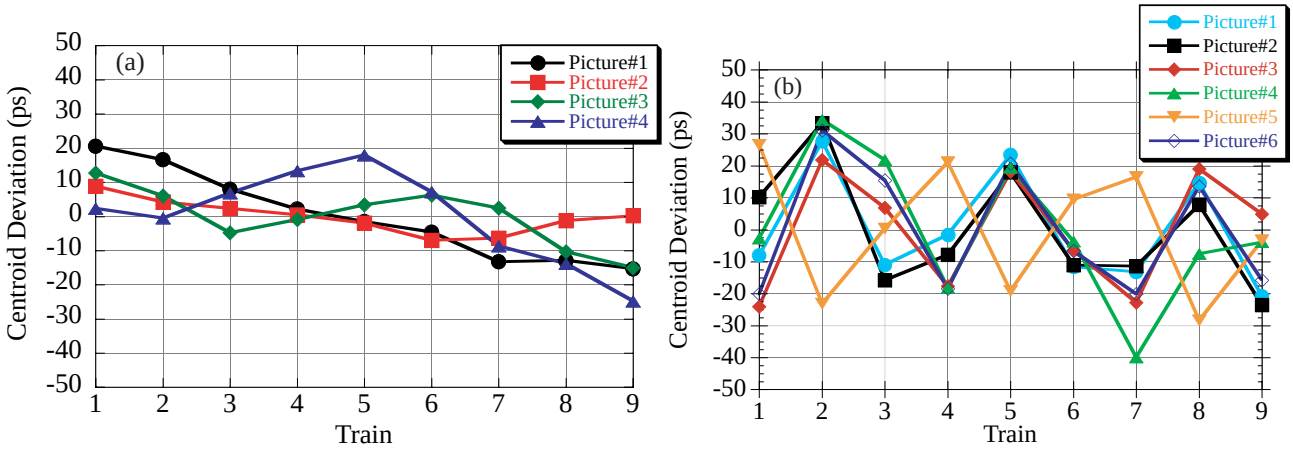

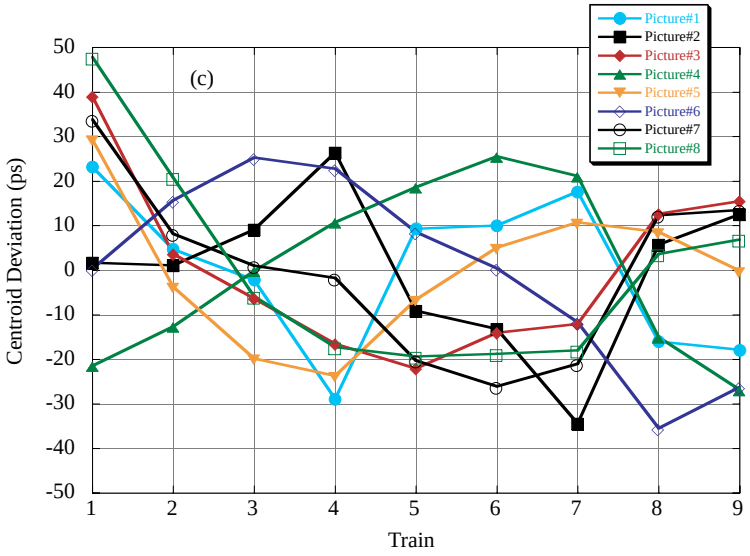

FIG. 28 (color). The train centroid deviation for (a) four images of 9 stable trains at 184mA total current, (b) six images of unstable trains at I=184mA total current and (c) eight images of unstable trains at 324mA total current.

(iii) When the instability is present, the average temporal spread for each train is longer. Figure 29 is the longitudinal train length with and without the instability present. Again the spread in the distribution has two components, one due to the bunch length and the other proportional to the dipole oscillation amplitude. If the entire increase in standard deviation is due to an oscillation amplitude $\hat{z}$

$$\frac{1}{2}\hat{z}^2 \cong \sigma^2_{\text{unstable train}} - \sigma^2_{\text{stable train}}$$

which gives a 8mm peak amplitude averaged over the measurements shown in fig. 29. In both cases the train temporal spread grows with current, but at each current, the train's temporal spread is larger with the instability present.

(iv) Time oscillations have been measured for both bunches and trains. Since train oscillations have been measured, the long-range wakefields have sufficient fields at subsequent trains to produce bunch-train instabilities.

(v) A comparison between bunch lengthening as a function of current, with a single bunch, or trains of bunches, is made. The growth rate with a single bunch present in CESR is $0.10\,\text{mm/mA}$, and the growth rate with multiple bunches is $0.21\,\text{mm/mA}$[7]. The growth rate is almost a factor of two larger for trains than bunches. This points out that the interbunch wakefields give a large contribution to bunch lengthening.

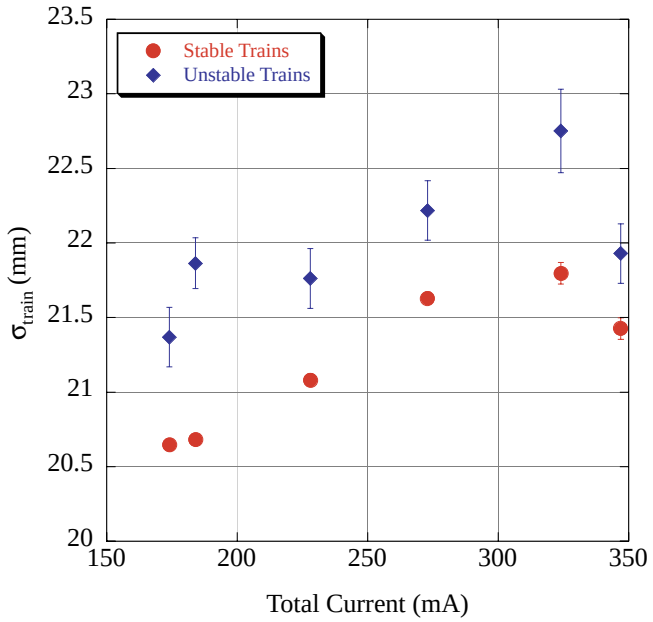

FIG. 29 (color). The temporal spread of the trains' with and without the instability present.

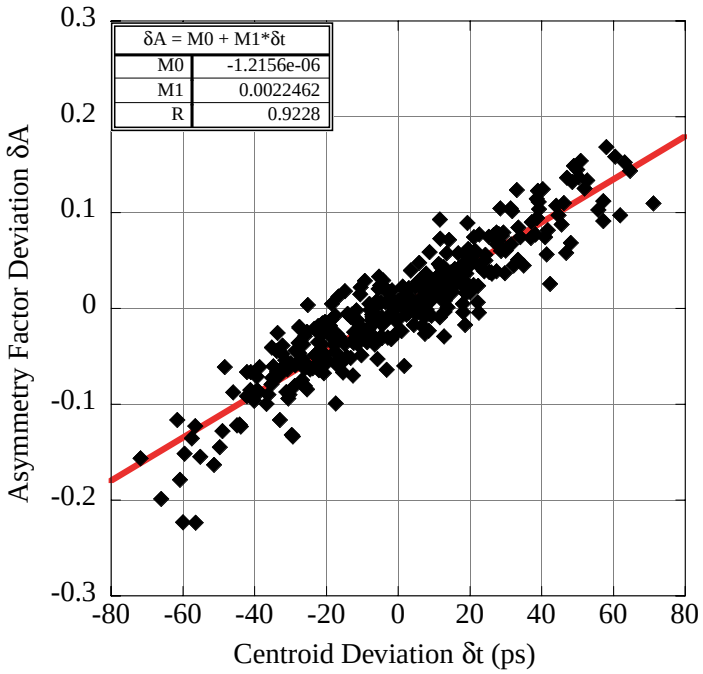

FIG. 30 (color). The change in the asymmetry factor as a function of centroid deviation when the trains are unstable.

The centroid deviation and asymmetry factor are highly correlated when the instabilities are present (figs. 30). This suggests the following: 1) If the train arrives early, the trains' asymmetry factor is negative (longer tail). It was pointed out in the previous section that a longer tail signifies bunches arriving early throughout the trains (an early arriving accordion mode). 2) A late arriving train refers to bunches arriving later throughout the train (a late arriving accordion mode). Figure 31 is a pictorial description of the dynamics in the train.

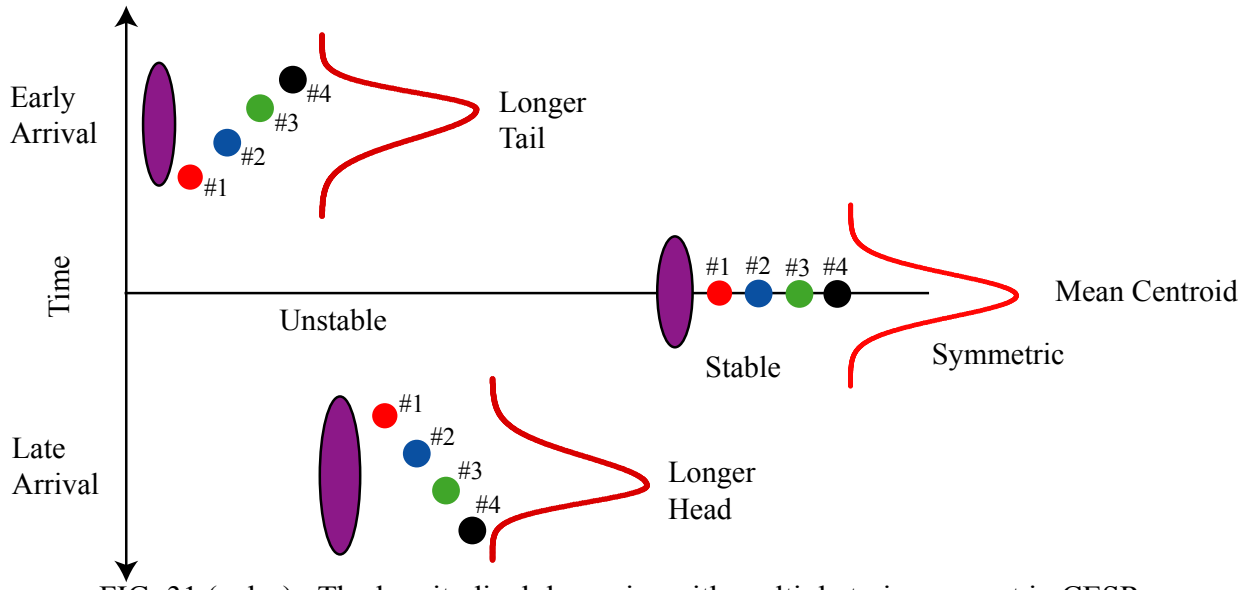

FIG. 31 (color). The longitudinal dynamics with multiple trains present in CESR.

C. Colliding Beam Motion

The primary mirror located in the CESR vacuum chamber, extracts synchrotron radiation for both electrons and positrons. Therefore, it is possible to view both beams with the streak camera simultaneously. Since the primary mirror is located diametrically opposite the Cornell detector (CLEO), the pair of adjacent trains observed by the streak camera is the pair of trains that collides in CLEO. Therefore, longitudinal time oscillations of colliding beams can be measured with the streak camera.

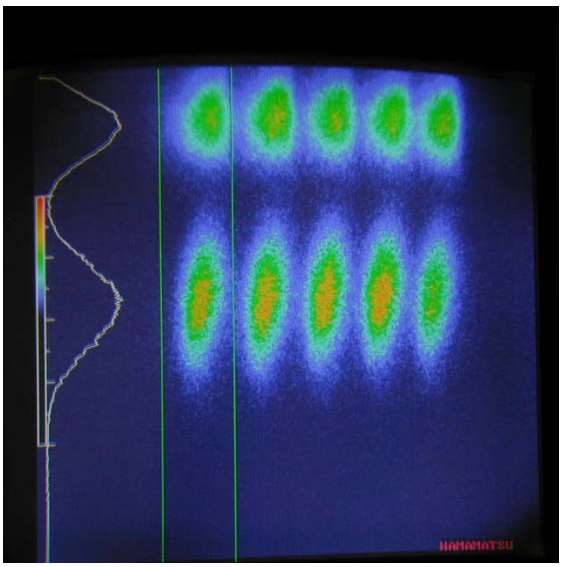

FIG. 32 (color). A typical streak camera image of stable colliding beams in CESR. Bunch one in the train is to the left and bunch five is to the right on the horizontal axis. The train on the top is positrons, and on the bottom are electrons. The longitudinal profile is on the left side of the figure. Under stable conditions, the bunches line up vertically.

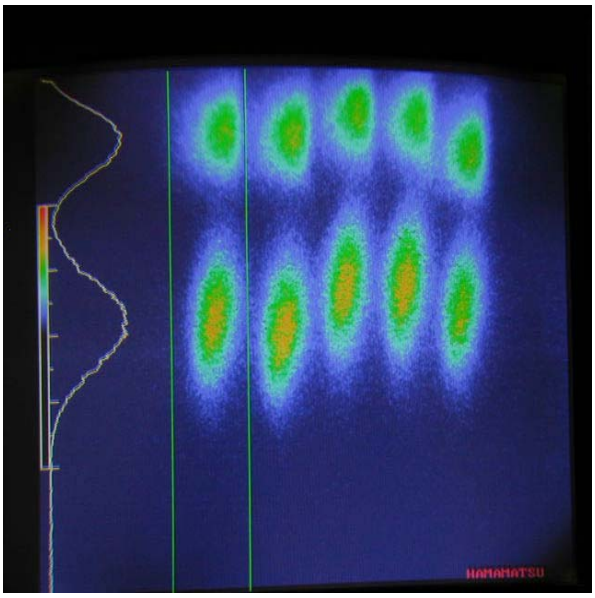

FIG. 33 (color). A typical streak camera images of unstable colliding beams in CESR. The bunches (same arrangements as fig. 32) in a train do not line up vertically.

A slight modification of the streak camera input optics was necessary to observe both bunches. This was accomplished by transporting the electron synchrotron radiation to the streak camera with an optical telescope. The positron synchrotron radiation was transported with the conventional optics.

The colliding beam experiment was performed during high-energy physics collisions when nine trains of five bunches of both electrons and positrons present in CESR. Streak camera images were taken when the bunches were unstable and stable. Typical representative images with stable (fig. 32) and unstable (fig. 33) motion with beams in collisions are presented.

Ideally, for stable collisions at the center of the CLEO detector, the time separation between bunches in the trains must remain constant. The goal of this experiment is to determine the time separation stability for colliding beams. The two different time oscillations, presented in the previous sections, measured for bunch collisions are: 1) train to train oscillations, and 2) bunch to bunch oscillations. Both oscillations require the following analysis of the longitudinal profiles.

For each image, the longitudinal profile of each colliding bunch (both electron and positron) is saved. Each profile is fit to a function that consists of two asymmetric Gaussian functions, one for each colliding beam. An example of a single profile fit to the two asymmetric Gaussian functions is displayed in fig. 34. The mean position for each function determines the time separation between bunches.

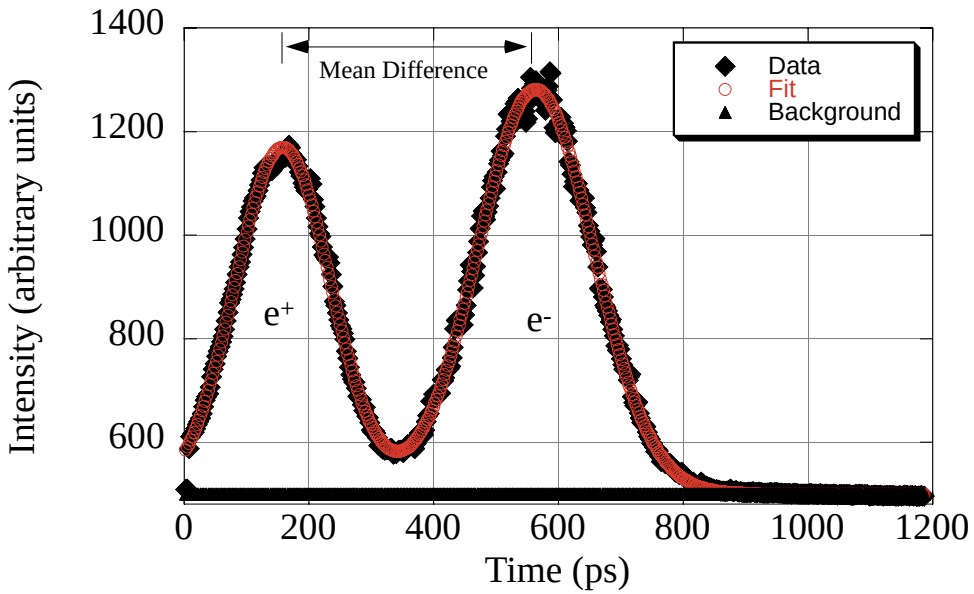

FIG. 34 (color). A single profile of the electron and positron bunches which collide at the interaction point. The longitudinal distributions are fit and the distance between the distributions is computed.

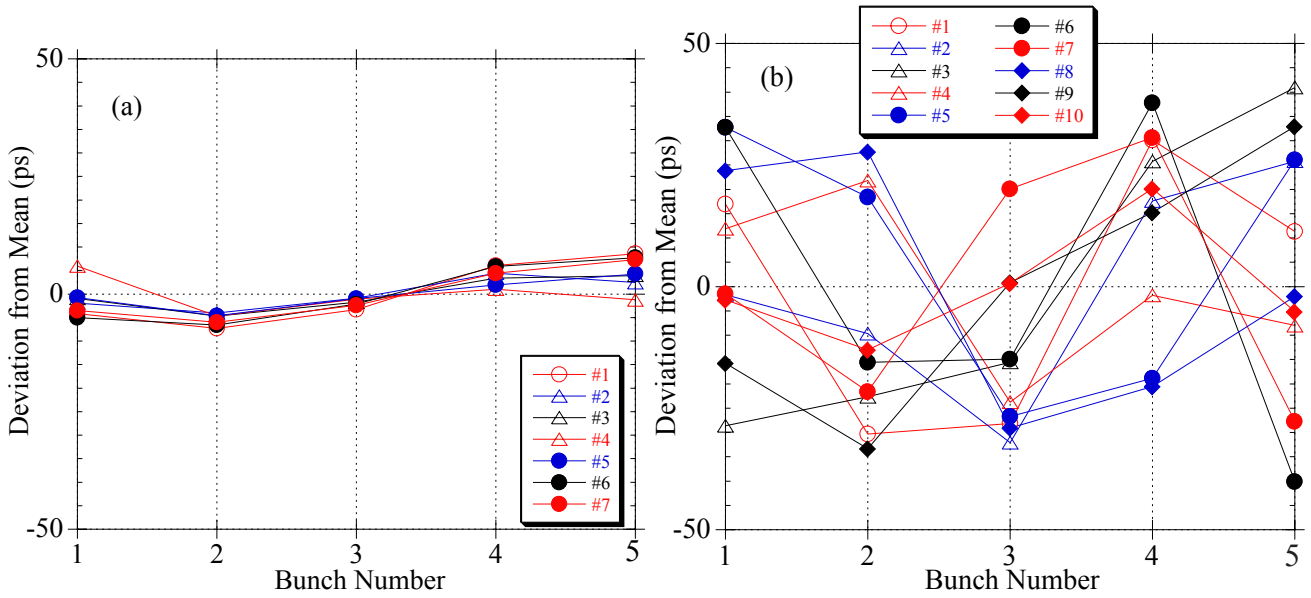

FIG. 35 (color). The residual from the mean location for the bunches in the train when the bunches are (a) stable and (b) unstable.

For train to train time oscillations, the oscillations are determined by computing the train centroid for each image, for both electrons and positrons. The difference of train centroids for electrons and positrons is the time separation for each train. The mean time separation changed by 6.6ps from stable to unstable collisions.

Bunch to bunch time oscillations are characterized by the standard deviation of the mean centroid for each train during stable and unstable collisions. The deviation from the mean position when

collisions are stable and unstable is displayed in fig. 35 for several streak camera images. The difference in the mean standard deviation between stable and unstable collisions is 29.6ps.

The luminosity degradation due to the longitudinal dipole-coupled bunch instability is estimated from the head on collision, "hourglass", calculations by Milton[6]. The time oscillation, from the bunch and train "hourglass" contributions, is 30ps or 9mm. This time oscillation changes the location of collision, and therefore increases the effective vertical betatron function, β_v^*. The reduction in luminosity from geometrical effects only due to the instability is given by the ratio of suppression factors

$$\frac{L_u}{L_s} = \frac{s_f(\sigma_z)_u}{s_f(\sigma_z)_s} = \frac{0.763}{0.814} = 0.94$$

The luminosity was measured by the CLEO detector during this experiment and is displayed in fig. 36. This reduction in luminosity measured by CLEO, approximately 24%, is substantially larger than the 6% estimated luminosity reduction from bunch and train time oscillations. A more detailed model including crossing angles and coupling from solenoid compensation is required to calculate an accurate estimate of luminosity reduction from the longitudinal oscillations.

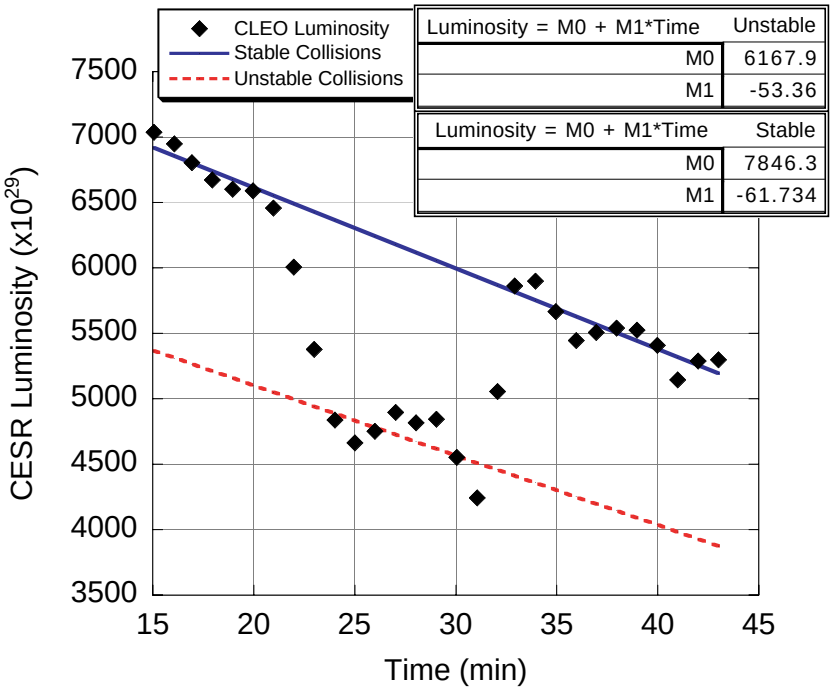

FIG. 36 (color). A plot of the CLEO luminosity as a function of time. The dip in the luminosity occurred when the longitudinal feedback system was turned off and the beams were unstable.

V. Conclusions

In this paper, we report the results of detailed measurements of the longitudinal dipole-coupled bunch instability at CESR. The measurements were made using a dual-sweep synchroscan streak camera. The experiments have allowed us to understand the longitudinal dynamics of the instability during high-energy physics collisions. The instability is damped by a strong feedback system that reduces its affect on luminosity and allows an increase in current threshold.

Measurements of single train, multiple trains and bunch collisions were performed. For a single train of bunches, we have concluded that: 1) above the instability threshold, the longitudinal feedback system stabilizes the temporal oscillations to approximately 5ps. Without feedback, the temporal oscillations have peak amplitudes of approximately 100ps. These oscillations, called bunch oscillations, degrade the High Energy Physics luminosity. 2) The oscillation modes within a train changes as a function of current. Just above the instability, an “accordion” mode of oscillation has been observed. The accordion mode has all the bunches in a train either moving together, or apart, in unison. At higher currents more complicated modes of oscillation are present. 3) The instability is less severe with the superconducting RF cavities. Previously, the instability would produce shape oscillations at high current and this would lead to beam loss[2]. The superconducting cavities have made significant difference in the characteristics of the instability. 4) These bunch oscillations change the asymmetry of the bunch distribution, which signifies a current flow in the bunch distribution. The asymmetry of the bunch distribution changes depending on its arrival time from a synchronous bunch. Figure 19 displays the change in bunches asymmetry as it oscillates in its potential well.

For multiple trains bunches in CESR, we have concluded that: 1) Trains have temporal oscillations, much like bunch oscillations, due to the longitudinal dipole-coupled bunch instability. These modes of oscillation can be represented as train modes. 2) Train to train centroid motion has been measured. The maximum train centroid oscillation is approximately 50ps with and 10ps without the instability. 3) Two modes of oscillation were measured, a period 3 and a combination of period 1 and 1.25 oscillation mode. 4) The average longitudinal distribution of the bunches in a train grows faster than the single bunch length as a function of current. This is due to the interbunch wakefields. 5) At large oscillation amplitudes, the train distribution is highly asymmetric and results in large "accordion" oscillations of the bunches in a train. A pictorial description of the time oscillation of trains and bunches is displayed in fig. 31.

Beam dynamics of colliding bunches were also measured. We can conclude from these measurements that: 1) the instabilities degradation of the luminosity is due to train and bunch oscillations. These oscillations reduce the luminosity by more than 20%. 2) A better model of CESR’s interaction region optical characteristics is required to estimate the luminosity reduction.

The operation of the dual sweep synchroscan streak camera is understood. The camera has provided detailed measurements of the longitudinal dynamics of the longitudinal dipole-coupled

bunch instability that could not be measured by a normal streak camera. The camera has proved to be a valuable diagnostic tool for characterizing beam oscillations and longitudinal beam dynamics for the Cornell Electron-Positron Storage Ring.

VI. Acknowledgments

The authors would like to thank the operation staff at the Laboratory of Nuclear Studies at Cornell University. We would also like to thank Robert Meller, David Rice, Robert Siemann, and Sasha Temnykh for useful discussions about the dynamics observed. This work was supported by the National Science Foundation.

VII. References

[1] Belomestnykh, S., et al., "Superconducting RF System for the CESR Luminosity Upgrade: Design, Status, Plans". SRF 960529-02.

[2] Holtzapple, R.L., et al., "Multiple Bunch Longitudinal Dynamics Measurements of the Cornell Electron-Positron Storage Ring ". Phys. Rev. ST Accel Beams 4, 014401, 2001.

[3] Sands, M., "The Physics of Electron Storage Rings: An Introduction", SLAC, SLAC-PUB-0121, Nov 1970. 172pp.

[4] Billing, M., "Observation of a Longitudinal Coupled Bunch Instability with Trains of Bunches in CESR," CLNS 98/1564.

[5] Chao, A.W., "Physics of Collective Beam Instabilities in High-Energy Accelerators", New York, USA:Wiley (1993) 371p.

[6] Milton, S., "Calculation of How the Ratio $\beta^* / \sigma_{\text{bunch length}}$ Affects the Maximum Luminosity Obtainable: The 'Hourglass Effect'.", Cornell University, Colliding Beam Note 89-1, 1989.

[7] Holtzapple, R.L. and Rice, D., "Single Bunch Longitudinal Measurements of the Cornell Electron-Positron Storage Ring with the Superconducting RF Cavities." Cornell University, Colliding Beam Note 01-1, 2001.

[8] Billing, M., "Modes of Oscillation of Trains of Bunches." Cornell University, Colliding Beam Note 99-2, 1999.